Mesoglobule Morphologies of Amphiphilic Polymers

E. A. Maresov and A. N. Semenov*

Université Strasbourg 1, Institut Charles Sadron, CNRS UPR 22, 23 rue du Loess, BP 84047, F67034 Strasbourg Cedex, France

Received June 5, 2008; Revised Manuscript Received September 5, 2008

ABSTRACT: A statistical theory of finite-sized aggregates and domain structures in dilute solutions of amphiphilic macromolecules (homopolymers or copolymers) is developed. A minimalist model involving, essentially, two types of chemical groups (insoluble H and soluble P) is studied in the regime where polymer tends to phase separate, forming rather dense amorphous particles with low surface energy. The surface tension and the elastic bending moduli of the polymer/solvent interface are obtained and are related to the molecular parameters. The Gaussian modulus κ_G is predicted to be negative; typically $|\kappa_G|$ is smaller than the mean bending modulus κ_2. It is shown that the condensed polymer phase can remain dense, homogeneous, and stable with respect to microphase separation even as the surface tension decreases down to zero (or below it). Stable large aggregates of well-defined size are predicted in this regime. The size of aggregates and their shape depend on surface tension γ, the spontaneous bending modulus κ_1, and the ratio κ_G/κ_2. We show that bicontinuous morphologies (rather than colloidally stable polymer mesoglobules) are thermodynamically favorable for small $|\kappa_G|$. We present a quantitative argument showing that the gyroid structure is more favorable than other bicontinuous morphologies (primitive cubic and double diamond). The $\gamma-\kappa_1$ phase diagrams showing the regions of stability of different morphologies are obtained. Two types of spherical mesoglobules are predicted, namely equilibrium and metastable globules whose sizes are shown to be essentially different: they depend on κ_1 in qualitatively different ways. Recent experimental data on mesoglobule formation in solutions of thermosensitive amphiphilic polymers are discussed in the theoretical light.

1. Introduction

Phase separation in simple fluids normally proceeds via formation of the condensed phase droplets that grow in size indefinitely. A similar process in polymer solutions can drive homopolymers to adopt compact globular states in poor solvent conditions.[1,2] However, homopolymer globules are not stable: they aggregate and form a macroscopic precipitate.[3,4] The aggregation is driven by the surface energy gain (the same driving force works for simple liquids causing fusion of small droplets).

Stabilization of finite polymer aggregates can be desirable for many reasons. Finding ways to control formation of well-defined polymer globules or stable aggregates can provide a basis for the development of functional polymeric materials exhibiting remarkable mechanical and structural properties similar to those of fine polymer emulsions or dispersions or block copolymer micelles in solution.[5,6] Well-defined nanoscale segregated polymer structures can also be used for the synthesis of membranes, molecular scaffolds, or microcapsules.

Other important examples of functional globules come from the biopolymer world: native folded proteins in stable compact state perform all sorts of useful tasks in living biological systems. The protein globules are stabilized by soluble shells of hydrophilic units normally present in the protein sequence.

A remarkable phenomenon was discovered recently: it was observed that a range of water-soluble homopolymers can form stable globules and mesoglobules in dilute solutions.[7,13,24,68] The relevant systems involve thermosensitive polymers that can undergo a heat-induced coil−globule transition near a lower critical solution temperature (LCST). This class of polymers includes poly(*N*-isopropylacrylamide) (PNIPAM), poly(*N*-cyclopropylacrylamide), poly(*N*-vinylcaprolactam) (PVCL), poly(vinyl methyl ether) (PVME), etc.[7,8,12−14,26] (see Figure 1). The polymers are soluble in cold water but phase separate at elevated temperatures, typically above 30−40 °C depending on their molecular weight and concentration.

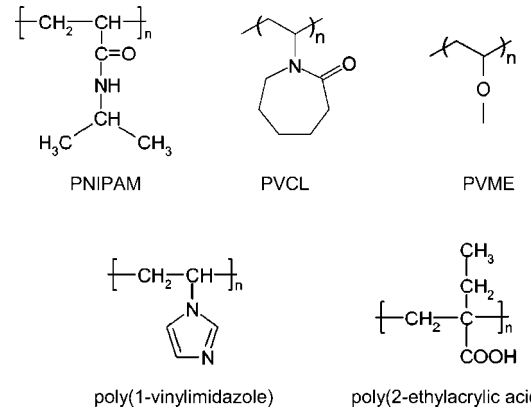

Figure 1. Examples of amphiphilic homopolymer chemical structures: poly(*N*-isopropylacrylamide) (PNIPAM), poly(*N*-vinylcaprolactam) (PVCL), poly(vinyl methyl ether) (PVME), poly(1-vinylimidazole), poly(2-ethylacrylic acid).

Repeat units of thermoresponsive homopolymers include both soluble and insoluble groups (for example, PNIPAM involves hydrocarbon main chain with hydrophilic amide groups in the side moieties). This feature justifies application of the term "amphiphilic homopolymers" to such systems.[15] The simplest model of an amphiphilic polymer involves just two types of chemical groups (monomer units or subunits): H (hydrophobic, insoluble) and P (polar, hydrophilic).[15,29,30] Possible structures of HP amphiphilic polymers are shown schematically in Figure 2.

It was recognized that the properties of amphiphilic homopolymers can be significantly different from those of classical homopolymers.[15] Noteworthy, many amphiphilic polymers (including thermosensitive homopolymers) are close to biopolymers in nature and behavior. Generally, amphiphilic polymers can serve as simple models for proteins and other biopoly-

* To whom correspondence should be addressed.

10.1021/ma801260g CCC: $40.75
Published on Web 11/12/2008

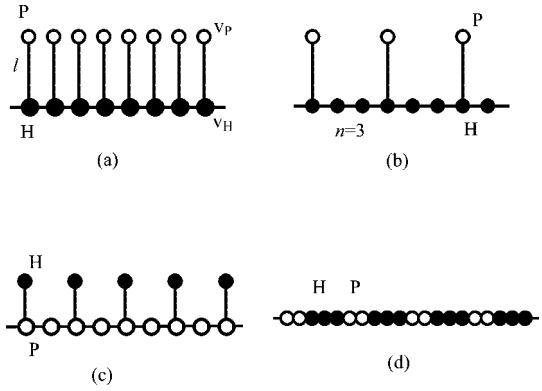

Figure 2. (a) Comb-like amphiphilic structure: each HP unit contains a hydrophobic group H (in the main chain) and a hydrophilic (soluble) P group attached to H. The volumes of H- and P-subunits are v_H and v_P, respectively; l is the length of HP spacer. (b) Similar structure with H-blocks (n H-units per one side P-group). (c) HP structure with hydrophobic side groups. (d) Linear HP polymer (a linear sequence of H- and P-blocks).

mers.[11,15] It is interesting, for example, that PNIPAM is homologous to the polypeptide poly(leucine). There is however an important difference: the vinyl polymer has a nonpolar backbone and includes peptide groups in its side chains, while poly(leucine) includes peptide groups in their backbone and have entirely nonpolar side chains.

Polyamphiphiles show remarkable surfactant properties and can exhibit conformational transitions induced by temperature or pH variation. For example, it was recently shown by computer simulations[15] that amphiphilic polymers can form stable condensed finite aggregates (globular structures of complicated shape). The simplest HP side-chain model (see Figure 2a) was analyzed. As the thermodynamic quality of the solvent decreases, the chain folds in a necklace-like conformation in which compact spherical beads ("pearls") of nearly equal size are connected by stretched chain fragments; the size of the pearls increases and their number decreases as the solvent becomes poorer. Finally, the pearls coalesce and form a sausage-like or a cylindrical-shaped particle.[15]

It is worth mentioning that amphiphilic polymers include an important class of polymer surfactants or polysoaps.[16] Typical polysoaps (including hydrophobically modified polymers) consist of a soluble backbone to which hydrophobic moieties are attached (see Figure 2c). Such polysoaps can be based on water-soluble thermosensitive polymers and can be used, for example, as associative thickeners (an important class of comb-like associating copolymers is based on polyacrylamide and its derivatives, including hydrophobically modified polyacrylamide). In the present paper we will focus on amphiphilic structures (shown in Figure 2a,b) with *side* hydrophilic groups and with relatively small ratio of the hydrophilic volume to the hydrophobic volume (like in tail-end-type polysoaps with grafted ionic groups; a synthetic approach leading to nonionic polyamphiphiles of that kind is considered in ref 61).

An HP amphiphilic polymer also bears similarity to a regular block copolymer in a selective solvent. It is well-known that such block copolymers can form stable aggregates—micelles.[5,17−22] Spherical and cylindrical micelles, as well as bilayer sheets and vesicles, are common. Noteworthy, however, the micelle size (radius, thickness) is typically of the order of the block size. In the case of amphiphilic homopolymers (see Figure 2a) it reduces to a monomer unit size, so only very thin lamellar sheets or vesicles, or cylindrical micelles (like cylindrical surfactant/polysoap wormlike micelles), are expected for HP homopolymer systems. Therefore, large stable globules and aggregates (mesoglobules) of amphiphilic homopolymers, as observed in experiments,[12,23−26,55,56] remain essentially unexplained.[69] This issue is considered theoretically in the present paper. Analyzing a simple model of amphiphilic polymers, we show that formation of *large* stable globules is possible and identify the relevant solution regimes.

Condensed states of polysoaps with *annealed* primary copolymer structure were investigated theoretically;[27] it was shown that while large globules of these polymers can be kinetically stable, they are never stable thermodynamically.

Globules of amphiphilic homopolymers with quenched structure (shown in Figure 2a) were the subject of another recent theoretical study.[28] The possible stability of homopolymer globules and mesoglobules was ascribed to the amphiphilic effect:[15] the presence of soluble P-units (that make the globule surface more hydrophilic)[13] can lead to a significant reduction of the globule surface tension which may cause stabilization of finite globules. The theory,[28] however, is not entirely satisfactory: it was overlooked there that the globule core would microphase separate and eventually disassemble in the relevant regime of low surface tension. Moreover, important bending energy contributions to the surface energy were not taken into account in ref 28 (see Discussion for more details).

The scope of the paper is as follows: The physical model is described in the next section, and then we calculate the surface energy and the surface bending moduli for the case of noninteracting P-groups; the effect of their interactions is considered in section 4; the condensed morphologies of amphiphilic polymers are analyzed in section 5, which is followed by the discussion of the main results.

2. The Model and the Free Energy

We consider a dilute solution of amphiphilic macromolecules adopting the side-chain HP model (see Figure 2a). Each polymer chain consists of an insoluble flexible backbone (H) to which a lot of short soluble fragments (P-groups) are grafted. The solvent is poor for the reference H-homopolymer involving only H-backbone. The soluble P-groups are connected to H-groups by rod-like spacers of length l. (A similar model of hydrophobic/hydrophilic polymers was studied in refs 15 and 28; more generally, the two-letter HP statistical mechanics models are widely used in protein research.[29−37]) The grafted HP amphiphilic homopolymer model (of the type shown in Figure 2a) roughly reflects the structure of such polymers as PNIPAM, PVCL, PVME, poly(1-vinylimidazole), and poly(2-ethylacrylic acid) (see Figure 1). We consider long polymer chains with $N \gg 1$ HP units.

It is assumed that the volume of the side fragment is dominated by the terminal P-group. Therefore, the rod-like spacers are considered as fantom: both volumeless and noninteracting. The hydrophobic backbone favors condensation of the HP-homopolymer in a dense globular state. We consider the most interesting general case: the polymer volume concentration inside the globule is $\phi_{pol} \sim 0.5$ (i.e., ϕ_{pol} is not assumed to be small). In this case the thickness of surface layer (at the polymer/solvent interface) is $\Delta \sim a_H$, where a_H is the H-group size (the volume of H-subunit is $v_H \sim a_H^3$). The minimal work required to transfer a whole polymer chain from condensed phase to the solvent is large ($\sim Nk_BT \gg k_BT$), so the polymer concentration in the solvent phase is very low.

Turning to the effect of P-groups, the general case $l \sim \Delta$ is hardly tractable with an analytical theoretical approach: some separation of length scales is necessary for a universal theoretical description to be applicable. We therefore focus on the case of long HP spacers: $l \gg \Delta$. (The condition $l^3 \gg v_H$ is similar in spirit to the condition $v/a^3 \ll 1$ imposed in the mean-field statistical theories of homopolymers.[3,4]) In addition, we demand that H-groups dominate by volume: $v_H \gg v_P$. In this case it is

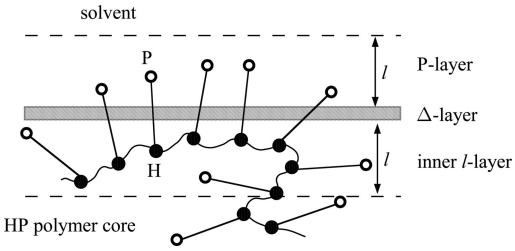

Figure 3. Schematic surface structure of amphiphilic polymer globule. The solvent/polymer interface involves three layers: P-layer (the outer l-layer with P-subunits), the Δ-layer (where concentration of H-subunits abruptly changes from c_0 to 0), and the inner l-layer (involving main-chain H-groups whose side HP bonds intersect the Δ-layer); $\Delta \ll l$.

natural to assume that polymer concentration and the structure in the bulk of the globule is only slightly affected by the presence of P-groups. For the start we neglect interactions *between* P-groups and postulate that backbone concentration c_H is constant inside the globule core: $c_H = c_0$ apart from a thin interfacial layer. (These approximations are lifted in section 4.)

Thus, a P-group can probe two environments: its molecular (chemical) potential is E_{in} inside the globule core and is E_{out} in the solvent outside the core (the probability that a P-unit is in the interfacial Δ-layer is neglected since $\Delta \ll l$).

$$\epsilon = E_{in} - E_{out} \tag{1}$$

$\epsilon > 0$ since P-groups like the solvent. Each time a P-group moves from polymer phase to the solvent, it gains the energy ϵ which can be small or large (compared with the thermal energy k_BT) depending on the HP chemical structure.

The simple model described above leads to the following free energy of an HP globule:

$$\mathcal{F} = \mathcal{F}_{ref} + E_{in}\mathcal{N}_{in} + E_{out}\mathcal{N}_{out} + F_{or} \tag{2}$$

Here $\mathcal{F}_{ref} = \mathcal{N}f_0 + \gamma_0\mathcal{A}$ is the free energy of the reference H-homopolymer globule (including the bulk term and the surface term, f_0 is the free energy per H unit in the homogeneous condensed polymer phase, $\mathcal{N}$ is the total number of units, γ_0 is the surface tension, $\mathcal{A}$ is the total surface area); $\mathcal{N}_{out}$ is the number of P-groups in the solvent (outside the globule core); $\mathcal{N}_{in} = \mathcal{N} - \mathcal{N}_{out}$; F_{or} accounts for the orientational entropy of HP bonds.

One may wonder (as one of the referees of this paper did) where the polymer connectivity is taken into account in the above equation. The answer is: it is relevant for the first *homopolymer* term in the r.h.s., $\mathcal{F}_{ref}$ (of course, the connectivity is also *implicitly* taken into account in the other terms: evaluation of $\mathcal{N}_{in}$ and $\mathcal{N}_{out}$ must be performed respecting the condition that l-bonds are emanating from the backbone H-units). Moreover, the well-known general theory of homopolymer globules (see, for example, refs 3 and 4) says that the chain connectivity is defining the *interfacial* structure of a large globule. The details of this structure, however, are irrelevant for the present model since the interfacial thickness $\Delta \sim a_H$ is assumed to be small (as compared to the HP bond length l). This is why the only relevant parameter that is affected by the chain structure is the reference H-homopolymer surface tension γ_0, which is treated as a known parameter (defined by temperature, solvent composition, etc.). In principle, eq 2 (with renormalized parameters) can be applied also to the system of unconnected HP units. However, in the first place, it is much less likely that unconnected units would form a condensed phase as their solubility is significantly enhanced due to their ideal-gas translational entropy.

Equation 2 can be rewritten as

$$\mathcal{F} = \text{const} + \gamma_0\mathcal{A} - \epsilon\mathcal{N}_{out} + F_{or} \tag{3}$$

where const represents the trivial bulk contribution which is simply proportional to the amount of polymer, $\mathcal{N}$.

The general eqs 2 and 3 are applicable also in the more general case when not every H-unit is modified (see Figure 2b). This case corresponds to an amphiphilic *co*polymer (like polysoap; there is however an important difference: the typical polysoap consist of a *hydrophilic* main chain with hydrophobic/amphiphilic moieties attached to it). Since Δ (the thickness of the surface layer where concentration of H-subunits changes from nearly c_0 to nearly 0) characterizes the unmodified hydrophobic homopolymer, the estimate $\Delta \sim a_H$ remains unchanged. However, if each n's H-subunit is modified, the two conditions imposed above (low volume fraction p of P-groups and long HP bonds) must be generalized as

$$p \equiv \frac{v_P}{nv_H} \ll 1, \quad l \gg \sqrt{n}a_H \tag{4}$$

Obviously, the case $n = 1$ corresponds to the amphiphilic homopolymer of Figure 2a.

3. Surface Energy

Let us consider a large HP globule with core size (radius) $R \gg l$. Apart from a trivial constant term its free energy is defined by the surface layer of thickness $\sim l$ adjacent to the Δ-interface (Figure 3): the grafted side rods (HP bonds) in this layer tend to orient toward the solvent, while farther inside the globule the bonds are oriented isotropically thus giving no contribution to the orientational free energy.

The total surface energy is $\mathcal{F}_s = \gamma_0\mathcal{A} + \Delta\mathcal{F}$, where $\Delta\mathcal{F}$ is the contribution due to P-groups ($\Delta\mathcal{F}$ depends on the surface curvature). The hydrophobic contribution γ_0 is considered as a constant since the Δ-layer is thin: $\Delta \ll l$. A more precise condition is worked out below; see eq 17.

The general expression for the surface energy $\Delta\mathcal{F}$ is derived below for the more general model of Figure 2b. The thin interfacial Δ-layer is considered as a geometrical surface dividing the system in two subvolumes: the uniform core (inner subvolume $\mathcal{V}_{in}$) and the solvent (outer subvolume $\mathcal{V}_{out}$). It is important that the modified H-subunits are nearly uniformly distributed in $\mathcal{V}_{in}$ since they are incorporated in the uniformly distributed H-backbone[70] and, moreover, are regularly arranged on the backbone, so that the distance between a modified subunit and the neighboring unmodified H-block is small (this distance is $\sim n^{1/2}a_H \ll l$, see the second condition (4)). Therefore, the grafted HP units can be considered as a system of "dipoles" whose H-ends are uniformly distributed in space (in $\mathcal{V}_{in}$). Each dipole is characterized by the position $\underline{r}$ of the "parent" H-end and the orientation (defined by the unit vector $\underline{n}_r$) of the HP bond. In order to find the free energy $\Delta\mathcal{F}$ associated with these dipoles, we consider the effective free energy of the system (the *effective Hamiltonian*)[67] $\mathcal{H}$ as a function of the set $\{\underline{n}_r\}$ of orientations of all HP dipoles (where $\underline{r}$, the position of the H-end of a dipole, runs over all modified H-subunits):

$$\mathcal{H}\{\underline{n}_r\} = \mathcal{F}_{ref} + E_{in}\mathcal{N}_P + \sum_r \epsilon_r$$

where $\mathcal{N}_P$ is the total number of HP dipoles and ϵ_r depends on the position $\underline{r} + \underline{n}_r l$ of the P-end of the dipole

$$\epsilon_r = \begin{cases} 0, & \text{if } \underline{r} + \underline{n}_r l \in \mathcal{V}_{in} \\ -\epsilon, & \text{if } \underline{r} + \underline{n}_r l \in \mathcal{V}_{out} \end{cases}$$

The total partition function of the system is (k_BT is considered as the energy unit here and below in this section):

$$Z_{tot} = \int \mathrm{e}^{-\mathscr{H}\{\underline{n}_r\}} \prod_r \mathrm{d}^2 n_r$$

Here $\mathrm{d}^2 n_r$ is the solid angle element divided by 4π (the 4π factor is introduced for convenience). The integrations are separated since P-groups do not interact (their interactions are taken into account in section 4). This way leads to the total free energy

$$\mathscr{F} = -\ln Z_{tot} = \mathscr{F}_{ref} + E_{int}\mathscr{N}_P - \sum_r \ln Z_r \qquad (5)$$

where Z_r is the orientational partition function of a dipole with H-end fixed at $\underline{r}$:

$$Z_r = \int e^{-\epsilon_r} \mathrm{d}^2 n_r = \int_{\underline{r}+\underline{n}l \in \mathscr{V}_{in}} \mathrm{d}^2 n + \mathrm{e}^{\epsilon} \int_{\underline{r}+\underline{n}l \in \mathscr{V}_{out}} \mathrm{d}^2 n \qquad (6)$$

(Note that $\int_{\underline{r}+\underline{n}l \in \mathscr{V}_{in}} \mathrm{d}^2 n + \int_{\underline{r}+\underline{n}l \in \mathscr{V}_{out}} \mathrm{d}^2 n = 1$.) It is the last term in the rhs of eq 5 that contributes to $\Delta\mathscr{F}$ (the second term is obviously irrelevant for the surface energy, and the surface part of the first term $\mathscr{F}_{ref}$ is merely $\gamma_0 \mathscr{A}$):

$$\Delta\mathscr{F} = -\sum_r \ln Z_r = -\psi_0 \int_{\underline{r} \in \mathscr{V}_{in}} \ln Z_r \, \mathrm{d}^3 r \qquad (7)$$

where $\psi_0 = c_0/n$ is concentration of the modified H-units (thus, $\psi_0 \mathrm{d}^3 r$ is the number of dipole H-ends in the volume $\mathrm{d}^3 r$).

The surface energy is calculated below for several important cases including plain, cylindrical, and spherical shapes of the core/solvent interface. In all these cases the surface energy per unit area of the interface is $f_s = \gamma_0 + \Delta f$, where $\Delta f = \Delta\mathscr{F}/\mathscr{A}$.

3.1. Plain Surface. In the case of plain core/solvent interface the dipole partition function Z_r depends only on the distance x from the H-end (located at $\underline{r}$) to the interface: $Z_r = Z(x)$. The surface energy contribution of P-groups, $\Delta f = \Delta\mathscr{F}/\mathscr{A}$, is therefore (see eq 7)

$$\Delta f = -\psi_0 \int_0^l \ln Z(x) \, \mathrm{d}x \qquad (8)$$

(Note that $Z(x) = 1$ for $x > l$; hence, there is no contribution to Δf coming from the region $x > l$.) Using eq 6, we get

$$Z(x) = 1 + \frac{\Omega}{4\pi}(e^{\epsilon} - 1)$$

where $\Omega = \Omega(x) = 2\pi[(l - x)/l]$ is the solid angle covered by the orientation $\underline{n}$ of an HP dipole whose H-end is fixed at x, while its P-end is located anywhere outside the globule core (i.e., the HP bond is intersecting the core/solvent interface located at $x = 0$).

Thus, we find the "amphiphilic" contribution to the surface tension $\gamma_P = \Delta f$ (for the *plain* core surface):

$$\gamma_P = -\psi_0 l f(\epsilon) \qquad (9)$$

where

$$f(\epsilon) = \frac{\mathrm{e}^{\epsilon} + 1}{\mathrm{e}^{\epsilon} - 1} \ln \frac{\mathrm{e}^{\epsilon} + 1}{2} - 1 \simeq \begin{cases} \epsilon/4, & \epsilon \ll 1 \\ \epsilon, & \epsilon \gg 1 \end{cases} \qquad (10)$$

Here and below we assume $\epsilon > 0$ (see eq 1; the case $\epsilon < 0$ is not interesting: it corresponds to $\gamma_P > 0$). The total surface tension

$$\gamma = \gamma_0 + \gamma_P = \gamma_0 - \psi_0 l f(\epsilon)$$

is decreasing with ϵ roughly linearly. As long as γ is positive, there is a free energy penalty for the globule surface, so fusion of globules (resulting in a surface area decrease) is favorable (finite globules/aggregates are unstable). Hence, it is important to figure out the conditions for γ to become negative. Typically $\gamma_0 \sim c_0 a_H$, so eqs 9 and 10 show that γ must vanish at $\epsilon = \epsilon_c \sim n a_H/l$. The critical energy parameter ϵ_c is therefore expected to be small, $\epsilon_c \ll 1$, if n is not large ($n \sim 1$); conversely, ϵ_c can be high for large n.

3.2. Curved Surfaces: Bending Energy. In the general case the polymer/solvent interface is curved. If the radius of curvature is large ($R \gg l$), the standard Helfrich approximation[51] is applicable: the surface energy (per unit area) $f_s = \gamma + f_{bend}$ can be expanded in terms of the principal curvatures C_1 and C_2:

$$f_s \simeq \gamma - \kappa_1(C_1 + C_2) + \frac{1}{2}\kappa_2(C_1 + C_2)^2 + \kappa_G C_1 C_2 \qquad (11)$$

where κ_1, κ_2, and κ_G are known as spontaneous, mean, and Gaussian bending moduli, respectively. In order to obtain these three moduli, it is sufficient to calculate the bending surface energy for weakly curved spherical and cylindrical surfaces. These calculations (outlined in the Appendices A and B) yield

$$\kappa_1 = \frac{\psi_0 l^2}{4}\left[\frac{3}{2} + 3\Lambda - (3\Lambda^2 - 1)\ln\frac{\mathrm{e}^{\epsilon} + 1}{2}\right] \qquad (12)$$

$$\kappa_2 = \frac{\psi_0 l^3}{8}\left[-2 + \frac{3}{2}\Lambda + 3\Lambda^2 - \frac{1}{2\Lambda} + 3\Lambda(1 - \Lambda^2)\ln\frac{\mathrm{e}^{\epsilon} + 1}{2}\right] \qquad (13)$$

$$\kappa_G = \frac{\psi_0 l^3}{12}\left[-\frac{2}{3} + \frac{7}{2}\Lambda + 7\Lambda^2 + \Lambda(3 - 7\Lambda^2)\ln\frac{\mathrm{e}^{\epsilon} + 1}{2}\right] \qquad (14)$$

where $\Lambda \equiv 1 + 2/(\mathrm{e}^{\epsilon} - 1)$. Thus, $\kappa_2 > 0$, while the other two moduli are always negative since $\epsilon > 0$. In what follows we focus on the cases of small and large ϵ; the results are simplified in these asymptotic regimes as

$$\kappa_1 \simeq -\psi_0 l^2 \epsilon^2/64, \quad \kappa_2 \simeq \psi_0 l^3 \epsilon/64, \quad \kappa_G \simeq -\psi_0 l^3 \epsilon/96, \quad \epsilon \ll 1 \qquad (15)$$

$$\kappa_1 \simeq \psi_0 l^2(-\epsilon/2 + 1.47), \quad \kappa_2 \simeq \psi_0 l^3/4, \quad \kappa_G \simeq \psi_0 l^3(-\epsilon/3 + 1.05), \quad \epsilon \gg 1$$

It is interesting that κ_1 is quadratic in ϵ for small ϵ, although this cannot be seen on the basis of a symmetry argument: obviously the cases $\epsilon > 0$ and $\epsilon < 0$ correspond to different surface structures.

The bending rigidities of the pure H-homopolymer interface can be estimated as

$$\kappa_1^{(H)} \sim \gamma_0 \Delta \sim c_0 a_H^2 \sim 1/a_H; \quad \kappa_2^{(H)} \sim \kappa_G^{(H)} \sim \gamma_0 \Delta^2 \sim 1 \qquad (16)$$

These homopolymer contributions are negligible (in comparison with the bending moduli due to P-groups, eqs 12−14) if

$$\psi_0 l^2 \gg 1/a_H \qquad (17)$$

This condition is adopted in the present paper.

4. Effect of Interactions of P-Groups

So far we neglected interactions of soluble P-groups. This is reasonable because their volume concentration is assumed to be small: $\phi_P = p\phi_H \sim p \ll 1$. More precisely, the density of free energy of P/P interactions in the second virial approximation outside the globule core is

$$F_{int} = \frac{1}{2}Bc_P^2$$

where $B \sim v_P$ is the virial coefficient. The corresponding contribution to the chemical potential $\partial F_{int}/\partial c_P = Bc_P \sim v_P c_P = \phi_P \ll 1$ is typically small. The interaction contribution must be compared to the bare molecular field contrast ϵ. Hence, the interactions can be neglected unless either ϵ is small ($\epsilon \ll 1$) or P/P interactions are strong for some reason, $B \gg v_P$. These two special cases are considered below.

4.1. Interaction Energy for $\epsilon \ll 1$. The situations inside and outside the globule core are considered separately. There are almost no H-groups outside the core (and outside the Δ-layer), so the interaction free energy density there is

$$F_{int} \simeq \frac{1}{2}Bc_P^2 - E_{out}c_P \tag{18}$$

where c_P is concentration of P groups (here and below we choose the volume of soluble group, v_P, as the unit volume, so c_P is simultaneously the volume concentration, $c_P = \phi_P$), and the second term accounts for P/solvent interactions.

In the core the interaction energy depends on both c_H and c_P: $F_{int} = F_{int}(c_H, c_P)$. Note that c_P changes significantly on the length scale l near the surface. The corresponding variation, δc_H, of c_H is relatively small ($\delta c_H \ll c_H$ since $\phi_P \ll \phi_H$; for example, if the P/H mixture is nearly incompressible, $\phi_H + \phi_P \simeq$ const, then $\delta\phi_H = \delta\phi_P \sim \phi_P$, so $\delta\phi_H/\phi_H \sim \phi_P/\phi_H \sim p \ll 1$), however its contribution to the free energy is non-negligible if $\epsilon \ll 1$. In the general case (allowing for some compressibility), it is the chemical potential of H-subunits, $\mu = \partial F_{int}/\partial c_H$, that is kept constant in the core, rather than the concentration c_H. (Note that μ is still not *exactly* constant: the force $-\nabla\mu$ can be balanced by the conformational contribution. An analysis shows, however, that this latter contribution is much smaller than $\mathcal{O}(\phi_P)$ and can be neglected if $\psi_0 \ll 1$ and $\epsilon \ll 1$.) It is therefore convenient to consider the thermodynamic potential $\tilde{F}(\mu, c_P) = F_{int} - c_H\mu$ instead of the free energy F_{int}. Expanding $\tilde{F}$ for small c_P:

$$\tilde{F}(\mu, c_P) \simeq \tilde{F}_0(\mu) - \tilde{E}(\mu)c_P + \frac{1}{2}\tilde{B}(\mu)c_P^2 \tag{19}$$

The free energy per H-group in the bulk macroscopic polymer phase is $f_{in} = F_{in}(c_0, \psi_0)/c_0$, where c_0 and $\psi_0 = c_0/n$ are concentrations of H- and P-groups, respectively, in the macroscopic phase. Subtracting the trivial bulk contribution $f_{in}\int c_H\, d^3r$ from the total interaction energy $\int F_{int} d^3r$, we get the surface energy:

$$\Delta\mathcal{F} = \int F_{int}^* d^3r \tag{20}$$

where

$$F_{int}^* = F_{int} - f_{in}c_H = \tilde{F} - \tilde{f}_{in}c_H \tag{21}$$

is the excess interaction energy density. Here

$$\tilde{f}_{in} = \tilde{F}(\mu, \psi_0)/c_0$$

The equilibrium osmotic pressure Π in the polymer phase must be zero:[71]

$$\Pi = c_P\frac{\partial\tilde{F}}{\partial c_P} - \tilde{F} = 0 \qquad \text{at } c_P = \psi_0$$

Using the last equation and eq 19, we get

$$\tilde{F}_0(\mu) = \frac{1}{2}\tilde{B}\psi_0^2, \quad \tilde{f}_{in} = \frac{1}{n}(\tilde{B}\psi_0 - \tilde{E}) \tag{22}$$

Next we recall that

$$c_H = -\frac{\partial\tilde{F}}{\partial\mu} \simeq c_0 + (c_P - \psi_0)\frac{\partial\tilde{E}}{\partial\mu} - \frac{1}{2}(c_P^2 - \psi_0^2)\frac{\partial\tilde{B}}{\partial\mu} \tag{23}$$

(Note that for incompressible core $c_H + c_P v_P/v_H =$ const; hence $\partial\tilde{E}/\partial\mu = -v_P/v_H$, $\partial\tilde{B}/\partial\mu = 0$.) On using relations 22 and 23 in eq 21, we get the effective free energy density *inside* the core:

$$F_{int}^* \simeq -E_{in}(c_P - \psi_0) + \frac{1}{2}B_{in}(c_P - \psi_0)^2 \tag{24}$$

where $E_{in} = (\tilde{E} - \psi_0\tilde{B})(1 + \delta)$, $B_{in} = \tilde{B} - (1/n)(\tilde{E} - \psi_0\tilde{B})(\partial\tilde{B}/\partial\mu)$, $\delta \equiv (-1/n)(\partial/\partial\mu)(\tilde{E} - \psi_0\tilde{B})$. Outside the core F_{int}^* coincides with F_{int} defined in eq 18.

The expression for the excess interaction energy F_{int}^* can be further simplified, noting that it is the integral, eq 20, that matters. The total number of H- and P-units are related:

$$\int c_P\, d^3r = \frac{1}{n}\int c_H\, d^3r$$

Therefore

$$\int_{in}\left(c_P - \frac{c_H}{n}\right)d^3r = -\int_{out} c_P\, d^3r \tag{25}$$

where $\int_{in}$ and $\int_{out}$ mean integrations inside and outside the core, respectively. On using eq 23, the integrand in the lhs becomes $c_P - c_H/n \simeq (1 + \delta)(c_P - \psi_0) + (1/2n)(\partial\tilde{B}/\partial\mu)(c_P - \psi_0)^2$. Thence, eq 25 can be rewritten as

$$\int_{in}(c_P - \psi_0)\, d^3r \simeq -\frac{1}{1 + \delta}\int_{out} c_P\, d^3r - \frac{1}{2n(1 + \delta)}\frac{\partial\tilde{B}}{\partial\mu} \times \int_{in}(c_P - \psi_0)^2\, d^3r$$

The last equation says that the total excess energy $\Delta\mathcal{F}$ would not change if we suppress the first term, $-E_{in}(c_P - \psi_0)$, in eq 24 and simultaneously appropriately renormalize both E_{out} and B_{in}. Applying these changes, we obtain an equivalent expression for the excess interaction energy density:

$$F_{int}^* \simeq \begin{cases} \frac{1}{2}B'(c_P - \psi_0)^2, & \text{inside the core} \\ -\epsilon c_P + \frac{1}{2}Bc_P^2, & \text{outside the core} \end{cases} \tag{26}$$

where

$$\epsilon = E_{out} - E_{in}/(1 + \delta) = E_{out} - \tilde{E} + \psi_0\tilde{B} \tag{27}$$

$$B' = B_{in} - \frac{1}{n(1 + \delta)}\frac{\partial\tilde{B}}{\partial\mu} = \tilde{B} + \frac{1}{n}\frac{\partial\tilde{B}}{\partial\mu}\left(\psi_0\tilde{B} - \tilde{E} - \frac{1}{1 + \delta}\right)$$

(For simplicity, we keep the same notation, F_{int}^*, in eq 26. Of course, eq 26 defines the renormalized F_{int}^* which is different from that defined in eq 24; it is the integral of F_{int}^* over the whole volume that does not change.)

The $-\epsilon c_P$ term as such was already taken into account (it corresponds to the $-\epsilon N_{out}$ term in eq 3; note however that ϵ is now renormalized as defined in eq 27). The other two terms in eq 26 involving B and B' represent the effect of P/P interactions. As H- and P-groups are incompatible, we expect that there is a *tendency* for their segregation also in the core, i.e., that $B' < 0$.

4.2. Interaction Contribution to Bending Moduli for $\epsilon \ll 1$. $\epsilon \ll 1$ means that there is a *weak* preference for a P-group to be outside the core (in the solvent phase). In this case it is reasonable to assume that the contribution of P/P interactions to the chemical potential of P-groups is also weak (i.e., to assume that $B\psi_0$ is small). Thus, for $\epsilon \ll 1$ we focus on the regime $B\psi_0 \ll 1$, $|B'| \sim B$ (note that, as shown below, $B\psi_0 \ll \epsilon$ is the most relevant and interesting regime). The above

conditions ensure that the molecular field $U = \partial F^*_{int}/\partial c_P$ is weak everywhere (since $U \sim B'\psi_0$ inside the core and $U \sim -\epsilon + B\psi_0$ outside; see eq 26); therefore, the distribution of P-groups is only slightly perturbed by the interactions. In other words, the B, B' interactions can be considered as a perturbation.

In the main approximation the interaction free energy $\Delta\mathcal{F}_{BB'} = \Delta\mathcal{F}_B + \Delta\mathcal{F}_{B'}$

$$\Delta\mathcal{F}_B = \frac{B}{2}\int_{out} c_P^2\, d^3r, \quad \Delta\mathcal{F}_{B'} = \frac{B'}{2}\int_{in}(\psi_0 - c_P)^2\, d^3r$$

where the integrals can be calculated using the unperturbed concentration profile (for $B = B' = 0$, $\epsilon = 0$). In this case, the two interaction contributions (outer and inner) are connected in a simple way: $\Delta F_{B'}$ can be obtained using an expression for $\Delta\mathcal{F}_B$ by replacing B with B' and changing the surface curvatures to the opposite. (This relation can be easily proved noting that $c_P \equiv \psi_0$ if the hydrophobic main chain uniformly fills the whole volume.)

Calculation of $\Delta\mathcal{F}_{BB'}$ for cylindrical and spherical globules is outlined in the Appendix C. Using the results obtained there (eqs C6, C7, C9, and C10), we find the interaction contributions to the surface tension ($\Delta\gamma_P$) and to the bending moduli ($\Delta\kappa_1$,...):

$$\Delta\gamma_P \simeq \frac{\psi_0^2 l}{24}(B + B'), \quad \Delta\kappa_1 \simeq \frac{\psi_0^2 l^2}{64}(B - B'),$$
$$\Delta\kappa_2 \simeq \frac{\psi_0^2 l^3}{320}(B + B'), \quad \Delta\kappa_G \simeq 0 \quad (28)$$

The spontaneous curvature bending modulus is

$$\kappa_1 \simeq -\frac{\psi_0 l^2}{64}\epsilon^2 + \frac{\psi_0^2 l^2}{64}(B - B') \quad (29)$$

The most interesting regime (where large distinct globules are formed, see the next section) corresponds to small positive κ_1 (see eq 36). On using eqs 29, 28, and 15 this regime can be specified as

$$\epsilon \gg B\psi_0 \gtrsim \epsilon^2 \quad (30)$$

The total surface tension for $\epsilon \ll 1$ is

$$\gamma = \gamma_0 + \gamma_P + \Delta\gamma_P \simeq \gamma_0 \simeq \gamma_0 - \frac{\psi_0 l\epsilon}{4} + \frac{\psi_0^2 l}{24}(B + B') \quad (31)$$

If $\kappa_1 = 0$, then the interaction contributions to γ, κ_2, and κ_G are subdominant, so $\kappa_2 \simeq \psi_0 l^3\epsilon/64$ and $\kappa_G \simeq -\psi_0 l^3\epsilon/96$ in the main approximation (see eqs 15). Hence

$$\left|\frac{\kappa_G}{\kappa_2}\right| \simeq \frac{2}{3} \quad (32)$$

in the relevant regime (30).

4.3. Bending Moduli for $\epsilon \gg 1$. We now turn to the rather special case of highly soluble P-groups with $B \gg \upsilon_P$. The large excluded volume B can be due to strong solvation effects or due to strongly elongated shape of P-groups. More precisely, we demand that $B\psi_0 \gg 1$. As before, we assume that the globule core is homogeneous (no microdomain structure); hence $B'\psi_0 \ll 1$ (see Appendix D, eq D3), and therefore P/P interactions in the core can be neglected: the molecular field inside is $U_P \equiv \partial F^*_{int}/\partial c_P \simeq 0$.

The second virial approximation may not be applicable in the regime $Bc_P \gg 1$. Hence, we generalize the second eq 26 as

$$F^*_{int} = -\epsilon c_P + \frac{1}{2}Bc_P^2 g(c_P/\psi_0)$$

where the factor $g(c_P/\psi_0)$ accounts for higher-order P/P repulsion interactions. We therefore expect that the g-function increases with c_P; it is also set $g(1) = 1$. The generalized molecular potential is

$$U_P = \frac{\partial F^*_{int}}{\partial c_P} = -\epsilon + Bc_P\left[g + \frac{1}{2}\frac{c_P}{\psi_0}g'\right] \quad (33)$$

where $g' = dg(z)/dz|_{z=c_P/\psi_0}$. Naturally, we still consider the regime when HP units near the surface (HP vectors) are oriented toward the solvent. Hence, U_P must be favorable ($U_P < 0$) outside. In view of eq 33, the latter condition leads to $\epsilon \gtrsim Bc_P$. Thence, we arrive at the condition $\epsilon \gtrsim B\psi_0 \gg 1$, as $c_P \sim \psi_0$ outside the core close to its surface.

The above conditions mean that not only $U_P < 0$, but also typically $|U_P| \gg 1$ in the outer l-layer (outside the core, see Figure 3). It is easy to show that therefore (i) nearly all HP units with main-chain H-groups in the inner l-layer have their P-groups in the outer l-layer; (ii) $U_P \simeq$ const in the outer l-layer, hence $c_P \simeq$ const there. (The second condition is backed by the following argument: Suppose that U_P is not nearly constant. This means that variation of U_P is $\gg 1$. Consider a small region where U_P has a maximum. P-groups must be expelled from this region since molecular potential there is much higher than on the average in the outer l-layer. Therefore, c_P must have a minimum in this region in contradiction with the assumed maximum of U_P: U_P must increase as a function of c_P; see eq 33.) The two conditions (i) and (ii) imply that concentration in the outer layer is

$$c_{out} \simeq \psi_0\frac{V_{in}}{V_{out}}$$

where V_{in} and V_{out} are the volumes of the inner and the outer layers, respectively (note that $c_H \simeq c_0$ inside the core including the inner layer; the small correction δc_H considered in section 4.1 is negligible here). Therefore, the interaction free energy due to the outer layer is

$$\Delta\mathcal{F} \simeq V_{out}F^*_{int}(c_{out}) \simeq -\epsilon\psi_0 V_{in} + \frac{B}{2}\psi_0^2\frac{V_{in}^2}{V_{out}}g\left(\frac{V_{in}}{V_{out}}\right)$$

The volumes (per unit area of the H/solvent interface) are $V_{in} = V_{out} = l$ for a plain interface. Hence, the surface tension is

$$\gamma \simeq \gamma_0 + \frac{\Delta\mathcal{F}}{\mathcal{A}} \simeq \gamma_0 - \epsilon\psi_0 l + \frac{B}{2}\psi_0^2 l$$

Note that the orientational entropy of HP units is disregarded here: its contribution to the tension is $\sim\psi_0 l$ and is negligible in the regime $\epsilon \gg 1$, $B\psi_0 \gg 1$. Calculating $\Delta\mathcal{F}$ also for cylindrical and spherical interfaces, we find the bending moduli:

$$\kappa_1 \simeq \frac{1}{2}l^2\psi_0\left[-\epsilon + \left(\frac{3}{2} + g'\right)B\psi_0\right],$$
$$\kappa_2 \simeq \frac{B\psi_0^2 l^3}{2}(2 + 4g' + g'') \quad (34)$$

$$\kappa_G \simeq \frac{l^3\psi_0}{6}(-2\epsilon + B\psi_0) \quad (35)$$

where $g' = dg(z)/dz|_{z=1}$, $g'' = d^2g(z)/dz^2|_{z=1}$ (good solvent conditions for P-subunits imply that both g' and g'' are positive). In particular, $\kappa_1 = 0$ if $(^3/_2 + g')B\psi_0 = \epsilon$. In this case $\gamma \simeq \gamma_0 - (1 + g')B\psi_0^2 l^3$, $\kappa_2 \simeq {}^1/_2(2 + 4g' + g'')B\psi_0^2 l^3$, $\kappa_G \simeq -{}^1/_3(1 + g')B\psi_0^2 l^3$

$$\left|\frac{\kappa_G}{\kappa_2}\right| \simeq \frac{1}{3}\frac{1+g'}{1+2g'+g''/2}$$

Therefore, $\kappa_G < 0$ and $|\kappa_G/\kappa_2| \lesssim 1/3$ in the strong interaction regime.

5. Results: Globule Morphologies and Phase Diagrams

5.1. The Regimes Considered. We are now in a position to analyze the equilibrium morphologies in solutions of amphiphilic polymers. The focus will be on the regimes where (i) the polymer tends to aggregate forming a condensed polymer phase with concentration c_0, coexisting with an almost pure solvent or, more precisely, with a dilute polymer solution (concentration c_d in the dilute phase is very low, $c_d \ll c_0$, and it is nearly independent of the mean concentration c; for simplicity, c_d is neglected in the present paper), (ii) the overall polymer volume fraction in the solution is small, and (iii) the characteristic length-scale L of the domain/globule structure is large: L is larger than the polymer/solvent interfacial thickness $\sim l$, $L \gg l$. The latter condition ensures that the excess polymer free energy can be written as a sum of volume and surface contributions:

$$\mathcal{F} \simeq \mathcal{F}_{vol} + \mathcal{F}_{surf}$$

where the volume term $\mathcal{F}_{vol}$ depends on the total amount of polymer (which is fixed) and on the osmotic pressure that is also fixed and is close to 0 in the dilute regime. Hence, $\mathcal{F}_{vol}$ does not depend on the shape of polymer domains (globules) and therefore can be considered as an irrelevant constant.

The surface term $\mathcal{F}_{surf}$ is generally defined as the integral of the surface energy density f_s over the whole polymer/solvent interfacial area. The energy f_s depends on surface curvatures: $C = C_1 + C_2$ (double mean curvature) and C_1C_2 (the Gaussian curvature); see eq 11. In the previous sections we analyzed how the coefficients (γ, κ_1,...) in the curvature expansion of f_s depend on the model parameters. Below in the present section we study how the polymer morphology depends on these coefficients.

The spontaneous curvature is $C_{ref} = \kappa_1/\kappa_2$; the corresponding radius of curvature, $L_{ref} = 1/|C_{ref}| = \kappa_2/|\kappa_1|$, defines the characteristic size $L \sim L_{ref}$. The applicability of the C-expansion in eq 11 is ensured by the condition $L \gg l$, which is equivalent to

$$l|\kappa_1|/\kappa_2 \ll 1 \tag{36}$$

This condition is satisfied for the model considered above, for example, for $\epsilon \ll 1$ and $B\psi_0 \ll \epsilon$.

The shape and size of polymer domains is defined by the condition $\mathcal{F}_{surf} = \min$. The minimization problem is complicated and is not tractable in the general case. Therefore, we will limit the analysis to the surfaces of constant mean curvature, $C = C_1 + C_2 = \text{const}$ (this is a rather standard approximation[38,39]). More precisely, we consider the following morphologies: spherical polymer droplets; polymer cylinders; modulated cylinders; plain layers; bicontinuous structures related to minimal surfaces (in particular, gyroid structures), and the corresponding inverse morphologies (Figures 4 and 5).

In all the relevant cases considered above, the Gaussian elastic modulus κ_G is negative (see eqs 14 and 35; the case $B\psi_0 > 2\epsilon \gg 1$ is irrelevant since the condition (36) is violated in this regime, see eqs 34). So, the consideration below is limited to the case $\kappa_G < 0$. In this case the modulated cylindrical morphology is never thermodynamically stable; see Appendix E. A similar analysis shows that globules in the form of spherocylinders (cylinders with semispherical caps), modulated spherocylinders, toroids, or disks are never thermodynamically stable as well (see ref 58 for comparison).

5.2. Bicontinuous Structures. The bicontinuous structures involve saddle-like polymer/solvent interfaces (with negative Gaussian curvature everywhere). We consider three classical bicontinuous morphologies with triply periodic interfaces of constant mean curvature:[38−40] "plumber's nightmare" (P), double-diamond (D), and gyroid (G); see Appendix F. Each of the three structures has cubic symmetry and involves two unconnected interwoven continuous networks of, say, polymer channels in a surrounding matrix (say, solvent matrix). The matrix always contains a surface of zero-mean curvature (minimal surface):[43] the Schwarz primitive (P), or the diamond (D) surface,[41] or the Schoen gyroid (G) surface.[42]

A discrimination between different bicontinuous morphologies is a difficult task, both theoretically and experimentally. Phase transitions between different bicontinuous surfactant mesophases often show no detectable enthalpy of transition,[44] indicating that these structures are characterized by nearly equal thermodynamic potentials. (The same feature is characteristic of block copolymer bicontinuous microdomain structures.[45]) Among different bicontinuous structures, it is the gyroid morphology that was most often identified experimentally in both block copolymer[40,46,47] and other systems.[48] For that reason we chose the gyroid as the bicontinuous structure to focus on in this paper. This choice is supported by the analysis (see below) showing that gyroid is indeed thermodynamically more favorable than the other bicontinuous structures in the regime, where the volume fraction of the matrix (which is bisected by the corresponding minimal surface) is low. This conclusion applies both to the direct structures (with solvent matrix) and to inverse structures (with polymer matrix).

5.3. Domain and Mesoglobule Structures for $\kappa_1 = 0$ and for $\gamma < 0$. The quadratic part of the surface energy reads

$$f^{(2)}_{bend} = \frac{1}{2}\kappa_2 C^2 + \kappa_G C_1 C_2$$

We demand that this quadratic form is positively defined (otherwise a polymer/solvent interface with low curvature is not stable), hence the condition

$$0 > \kappa_G > -2\kappa_2 \tag{37}$$

This condition is always satisfied (in the relevant regime of small $|\kappa_1|$) for the HP polymer model considered above.

The linear term is $-\kappa_1 C$. It is the case of sufficiently small $|\kappa_1|$ that is considered as explained above (see eq 36). The very point where the spontaneous curvature vanishes, $\kappa_1 = 0$, is not so interesting, however. In this case a plane interface is always more favorable than a curved one, so the polymer molecules either precipitate forming a homogeneous macroscopic phase (if $\gamma > 0$) or self-assemble in thin layers (that can also transform to closed vesicles) if $\gamma < 0$. In the latter case the layer thickness h tends to $2l$ if $|\gamma| \to 0$; h decreases with $|\gamma|$. For example, for small $\epsilon \ll 1$, the surface tension is $\gamma \simeq \gamma_0 - \psi_0 l\epsilon/4$ (see eq 31; the B-term there is negligible in view of the condition $\kappa_1 = 0$), and the optimal layer thickness is

$$h \simeq 2l, \quad \gamma < 0, \quad |\gamma| \ll \psi_0 l\epsilon$$

$$h \simeq 2l\sqrt{\frac{\gamma_0}{\psi_0 l\epsilon}}, \quad \gamma < 0, \quad \gamma_0 \ll \psi_0 l\epsilon$$

The same morphology (layers/vesicles) is stable also for small κ_1 if $\gamma < 0$ (the condition (36) is assumed as before). The reason is simple: although interfacial curvature is favorable for $\kappa_1 \neq 0$, a nonlamellar domain structure with near-optimally curved surfaces necessarily implies large domain size (since spontaneous curvature is small) and hence low surface-to-volume ratio, which is unfavorable as the surface tension is negative.

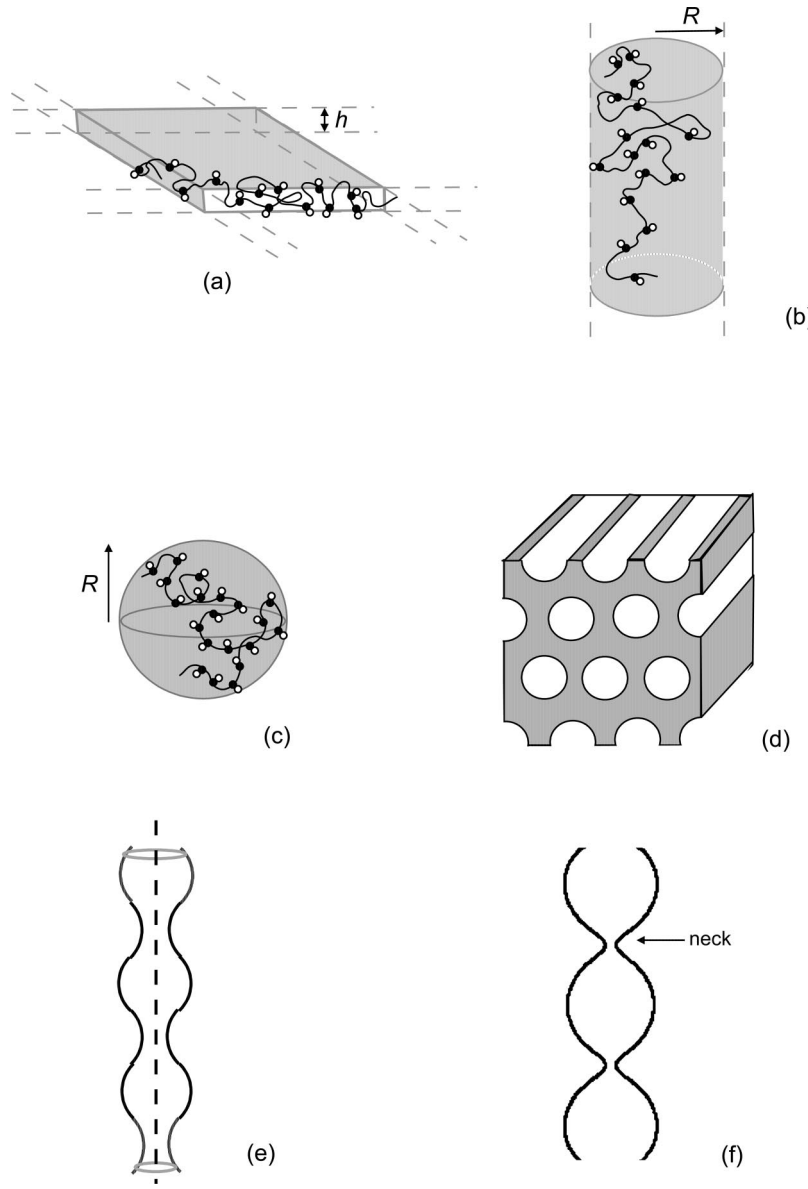

Figure 4. Amphiphilic polymer morphologies: (a) thin polymer layer (lamella of thickness h); (b) cylindrical aggregate; (c) spherical aggregate; (d) inverse cylindrical structure (hexagonal array of solvent cylinders in polymer matrix); (e) modulated cylinder; (f) nearly spherical beads connected by thin necks.

The remaining regimes, $\kappa_1 \neq 0$ and $\gamma \geq 0$, are more interesting and are considered below.

5.4. Morphologies for $\gamma = 0$ and $\kappa_1 > 0$. For $\gamma = 0$, both the macroscopic polymer condensed phase and a structure of lamellar layers are characterized by zero surface free energy, and both states are less favorable than one of the domain structures considered below.

It is convenient to use reduced variables considering the reference length-scale $L_{ref} = \kappa_2/|\kappa_1|$ and the energy $E_{ref} = \kappa_2$ as the corresponding (length, energy) units. (Note that the thermal energy k_BT is irrelevant in this section: any thermal fluctuations are not considered here. This is plausible since $\kappa_2 \gg k_BT$ as follows from the condition (17) which ensures that $\psi_0 l^3 \gg 1$.)

The (reduced) surface free energy density (for $\gamma = 0$ and $\kappa_1 > 0$) is

$$f_s \simeq -C + \frac{1}{2}C^2 - \kappa C_1 C_2 \tag{38}$$

where $\kappa = -\kappa_G/\kappa_2$ is the reduced Gaussian elastic modulus ($\kappa > 0$ as $\kappa_G < 0$). For cylindrical aggregates (mesoglobules) $C_1C_2 = 0$, so the free energy per unit volume is $F_{cyl} = (-C + {}^1/_2C^2)A/V$, where $C = 1/R$, R is the cylinder radius, and the surface-to-volume ratio $A/V = 2/R$, so $F_{cyl} = -C^2(2 - C)$. Minimizing it, we get

$$C = 4/3, \quad F_{cyl} = -32/27$$

For spherical aggregates of radius R, $C = 2/R$, $C_1C_2 = C^2/4$, and $F_{sph} = {}^3/_2C(-C + [(2 - \kappa)/4]C^2)$, so the free energy minimum corresponds to

$$C = \frac{8}{3(2-\kappa)}, \quad F_{sph} = -\frac{32}{9(2-\kappa)^2}$$

The transition between spherical and cylindrical morphologies occurs when $F_{cyl} = F_{sph}$, i.e., at $\kappa = 2 - \sqrt{3} \approx 0.27$. At the transition point the cylinder radius $R_{cyl} = 3/4$ and the sphere radius is $R_{sph} = 3\sqrt{3}/4$; i.e., the radius increases by the factor $\sqrt{3}$ as κ rises across the transition.

Let us turn to the gyroid morphology (see Figure 5 and Appendix F). The condensed polymer occupies the volume inside the channels. For simplicity, we consider a primitive cell

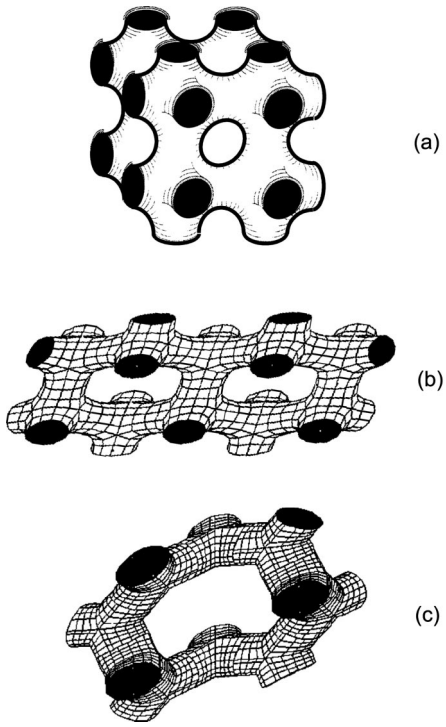

Figure 5. Constant mean curvature (CMC) surfaces: (a) primitive P; (b) diamond D; (c) gyroid G. Direct bicontinuous morphologies (of P, D, or G type) involve two equivalent unconnected interwoven triply periodic networks of polymer channels bounded by the corresponding CMC surfaces (in the case of gyroid the second network is the mirror image of the first one). The networks are surrounded by the polymer matrix. In the inverse morphologies the polymer and solvent regions are interchanged.

of just one gyroid network (the second network is equivalent); the primitive cell volume is $V_{cell} = L^3$, where L is its characteristic size. The free energy per unit volume of polymer phase in the channels is

$$F_{gyr} = \frac{1}{V}\int f_s \, dA = \frac{A}{V}(-C + C^2/2) - \kappa\frac{2\pi n_E}{V} \qquad (39)$$

where $n_E = -4$ is the Euler−Poincare characteristic of the polymer/solvent interface in the primitive gyroid cell, $V = \phi V_{cell} = \phi L^3$ is the polymer volume, $A = \bar{A}L^2$ is the surface area, and $C = \bar{C}/L$ is the (doubled) surface mean curvature. The dimensionless surface area $\bar{A}$, curvature $\bar{C}$, and volume fraction ϕ are parameters characterizing the family of constant-mean-curvature gyroid surfaces; the three parameters are related as outlined in Appendix F. Minimization of F_{gyr} with respect to L yields

$$F_{gyr} = -\frac{16}{27}\frac{\bar{A}}{\bar{C}\phi}\left(1 + \frac{16\pi\kappa}{\bar{A}\bar{C}^2}\right)^{-2}, \quad C = \frac{4}{3}\left(1 + \frac{16\pi\kappa}{\bar{A}\bar{C}^2}\right)^{-1}$$

Minimizing F_{gyr} further along the family of gyroid surfaces (i.e., essentially, with respect to ϕ), we get the gyroid free energy as a function of κ. The results show that gyroid and cylindrical morphologies can coexist ($F_{gyr} = F_{cyl}$) at $\kappa \approx 0.118$. At the transition point $\phi = 9.4\%$, $C = 1.23$, $L = 5.5$ in the gyroid phase, and $C = 4/3$ in the cylinder phase. Thus, gyroid is stable for $\kappa < 0.118$; cylinders—for $0.118 < \kappa < 0.27$; spheres—for $\kappa > 0.27$.

The κ-dependencies of the gyroid cell size L, its interface curvature C, and the single-network volume fraction ϕ are shown in Figure 6. Note that the parameters show a fast variation around $\kappa \sim 0.1$. The reason is that F_{gyr} in this region shows a very flat minimum as a function ϕ. (The optimum ϕ and other parameters in this region are also very sensitive to a numerical error in the $\bar{C}(\phi)$ dependence.) The curvature C is nearly constant increasing from $C = 1$ at $\kappa \to 0$ to $C = 1.23$ at the transition point. The (reduced) cell size is decreasing significantly for small κ:

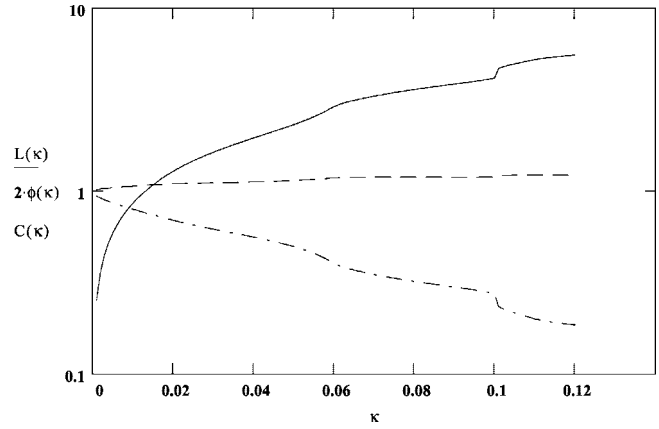

Figure 6. Dependencies of the reduced cell size L of gyroid structure (solid line), of the reduced interfacial curvature C (dash), and of the double-network volume fraction 2ϕ (dash-dot) on the reduced Gaussian modulus κ.

$$L \simeq 7.84\sqrt{\kappa}, \quad \kappa \ll 1$$

Note that due to twin gyroid networks the total fraction of polymer channels in the gyroid phase is 2ϕ. This fraction changes from 18.8% at the transition point ($\kappa \approx 0.118$) to almost 100% for $\kappa \ll 1$. The volume fraction of solvent matrix, ϕ_m, in the gyroid phase in the latter regime is

$$\phi_m = 1 - 2\phi \simeq 1.76\sqrt{\kappa}, \quad \kappa \ll 1$$

The *mean* polymer concentration in the gyroid phase is $c_{gyr} = 2\phi c_0$. The mean polymer concentration in the whole system, c, is assumed to be very small: $c < c_{gyr}$ (recall that $2\phi \gtrsim 0.2$ and that c_0 is not small). Hence, the system must separate in two macroscopic phases for $\kappa < 0.118$: the microdomain gyroid phase and the nearly pure solvent. By contrast, for $\kappa > 0.118$ the system is macroscopically homogeneous and can be considered as a colloidal solution of polymer spheres or cylinders.

Let us return to the issue of thermodynamic stability of gyroid morphology vs other bicontinuous structures. This problem can be easily analyzed in the regime of low ϕ_m (i.e., for $\kappa \ll 1$). In this regime the reduced free energy of a bicontinuous structure can be written as (compare with eq 39)

$$F_{bicont} \simeq \frac{\bar{A}}{\phi}\frac{1}{L}(-C + C^2/2) + \frac{8\pi\kappa}{\phi L^3}$$

where $\phi \simeq 0.5$ and $\bar{A} = \bar{A}(\phi) \simeq \bar{A}(0.5)$ (thus $\bar{A}$ is the area of the *minimal* surface inside a primitive cell of $V_{cell} = 1$, see eq F1). The minimizations of F_{bicont} with respect to C and L are formally decoupled in this regime, yielding $C \simeq 1$, $L \simeq (48\pi\kappa/\bar{A})^{1/2}$, and

$$F_{bicont} \simeq -\frac{1}{6\sqrt{3}}\frac{\bar{A}^{3/2}}{\kappa^{1/2}}$$

Therefore, the free energy depends on the reduced area $\bar{A}$. The largest area $\bar{A}$ (i.e., the lowest F_{bicont}) corresponds to the gyroid (see eq F1). Hence, the gyroid is the most stable among the bicontinuous structures.[72]

5.5. Inverse Morphologies for $\gamma = 0$, $\kappa_1 < 0$. If $\kappa_1 < 0$, the spontaneous curvature is negative, i.e. a concave interface is

favored. In this case inverse structures of solvent-filled spheres, or cylinders, or gyroid channels in the polymer matrix are expected.

In particular, the inverse cylindrical structure involves a system of parallel solvent cylinders. The cylinders must be *nearly close-packed* (*close-packed*, because minimization of the free energy per unit volume of condensed polymer demands minimization of the volume occupied by polymer matrix; *nearly*, because there must be a polymer layer between the neighboring cylinders); hence, they form a 2-dimensional hexagonal lattice. The volume fraction of the polymer matrix is $\phi_m \simeq 1 - \pi/(2\sqrt{3}) \approx 0.093$, and the surface-to-volume ratio is $A/V = \alpha_{cyl}C$, where $C = 1/R$ is the interfacial curvature (R, the cylinder radius)

$$\alpha_{cyl} = \frac{2\pi}{2\sqrt{3} - \pi}$$

The reduced surface free energy density is still defined in eq 38 (with length and energy units, L_{ref} and E_{ref}, defined in the previous section and with the opposite sign of the interfacial curvature C: we redefine $C \rightarrow -C$ viewing the curvature from the opposite side of the surface).

The free energy minimization yields

$$F_{cyl} \simeq -\frac{16}{27}\frac{2\pi}{2\sqrt{3} - \pi}, \quad C = 4/3$$

The inverse spherical structure can be analyzed in a similar way, assuming a nearly close-packed arrangement of solvent spheres of radius R. The polymer matrix volume fraction is $\phi_m \simeq 1 - \pi/(3\sqrt{2}) \approx 0.26$; $A/V \simeq \alpha_{sph}C$, $C = 2/R$

$$\alpha_{sph} = \frac{2\pi}{4\sqrt{2} - 4\pi/3}$$

The optimum parameters are

$$C_{sph} \simeq \frac{8}{3(2 - \kappa)}, \quad F_{sph} \simeq -\frac{64}{27(2 - \kappa)^2}\alpha_{sph}$$

For the inverse gyroid structure, the volume fraction of polymer matrix is $\phi_m = 1 - 2\phi$, the volume of condensed polymer in one cell is $V = (1 - 2\phi)L^3$, the corresponding interfacial area is $A = 2\bar{A}L^2$, and the curvature $C = \bar{C}/L$. The free energy per unit volume of condensed polymers is

$$F_{gyr} = \frac{A}{V}(-C + C^2/2) + \frac{8\pi\kappa}{V/2}$$

Minimization of F_{gyr} with respect to L yields

$$L = \frac{3}{4}\bar{C}\left(1 + \frac{16\pi\kappa}{\bar{A}\bar{C}^2}\right), \quad F_{gyr} = -\frac{16}{27}\frac{\bar{A}}{(0.5 - \phi)\bar{C}}\left(1 + \frac{16\pi\kappa}{\bar{A}\bar{C}^2}\right)^{-2}$$

Minimizing further the free energy with respect to ϕ, we find that inverse gyroid is stable for $\kappa < \kappa_{gc} \approx 0.0136$. The inverse cylindrical structure is favored at higher κ, for $\kappa_{gc} < \kappa < \kappa_{cs} \approx 1.06$; the inverse spherical structure is predicted for $\kappa > \kappa_{cs}$. At the gyroid/cylinder transition point $\phi \approx 0.44$, $\phi_m \approx 12\%$, $L \approx 0.79$, and $C \approx 0.66$ in the gyroid structure; $C \approx 1.33$ for cylinders, and C further increases up to $C \approx 2.84$ in the spherical phase at $\kappa = \kappa_{cs}$. The volume fraction of polymer matrix in all the inverse microdomain structures is $\phi_m \gtrsim 0.1$ (except for $\kappa \ll 0.01$). Therefore, in all the inverse regimes the system is expected to show macroscopic phase separation, i.e., almost pure solvent in coexistence with one of the microdomain phases.

The above treatment of the inverse gyroid structure can be simplified: the dependence $\bar{C}$ on ϕ can be approximated by the linear relationship $\bar{C} \simeq c(0.5 - \phi)$ as ϕ is close to 0.5. Here $c \equiv -\mathrm{d}\bar{C}/\mathrm{d}\phi|_{\phi=0.5}$ is a constant. Simultaneously, $\bar{A}$ can be approximated by the *minimal* area $\bar{A}$ for $\phi = 0.5$. Thus, we get

$$F \simeq -\frac{c}{27}\frac{\bar{A}^2}{4\pi}\frac{1}{\kappa}, \quad C \simeq 2/3, \quad \phi_m \simeq \frac{8\sqrt{\pi}}{c\sqrt{\bar{A}}}\sqrt{\kappa}, \quad L \simeq \frac{6\sqrt{\pi}}{\sqrt{\bar{A}}}\sqrt{\kappa} \tag{40}$$

These equations are accurate in the whole region of inverse gyroid (with $c \approx 8.9$, $\bar{A} \approx 2.4533$). Thus, both ϕ_m and L are proportional to $\sqrt{\kappa}$; this behavior is similar to that predicted for the direct gyroid structure for small κ.

Moreover, eqs 40 are applicable also to other bicontinuous inverse morphologies (with different constants c and $\bar{A}$). Obviously, the most favorable structure must correspond to the highest $c\bar{A}^2$. Using eqs F1 and F3 leads to $c\bar{A}^2 \approx 52.0$ (for P-family), 52.2 (for D-family), and 53.5 (for G-family). Therefore, it is the inverse gyroid morphology that is favored.

5.6. The General Case: $\gamma \geq 0$. Phase Diagrams. The case of positive surface tension of plain polymer/solvent interface can be considered in exactly the same way as the case $\gamma = 0$ analyzed above. The key results only are provided below. The surface free energy density for $\kappa_1 > 0$ is

$$f_s = \bar{\gamma} - C + C^2/2 - \kappa C_1 C_2$$

where we use the reduced variables as before, with length and energy units $L_{ref} = \kappa_2/|\kappa_1|$ and $E_{ref} = \kappa_2$ (thus, in particular, $\bar{\gamma} = \gamma\kappa_2/\kappa_1^2$).

For the direct cylindrical structure we find

$$C = L_{ref}/R = \frac{1}{3}(2 + \sqrt{4 - 6\bar{\gamma}}),$$
$$F_{cyl} = \frac{4}{27}\left[9\bar{\gamma} - 4 - 4\left(1 - \frac{3\bar{\gamma}}{2}\right)^{3/2}\right], \quad \bar{\gamma} < \frac{1}{2} \tag{41}$$

For the direct spherical structure

$$C/2 = L_{ref}/R = \frac{1}{3}\frac{2 + \sqrt{4 - 3\bar{\gamma}(2 - \kappa)}}{2 - \kappa},$$
$$F_{sph} = C(\bar{\gamma} - C/2), \quad \bar{\gamma} < \frac{1}{2 - \kappa} \tag{42}$$

For the direct gyroid structure

$$C = \frac{2 + \sqrt{4 - 6\bar{\gamma}\mu}}{3\mu}, \quad F_{gyr} = \frac{\bar{A}}{\phi\bar{C}}\frac{C}{3}(2\bar{\gamma} - C), \quad \bar{\gamma} < \frac{1}{2\mu} \tag{43}$$

where $\mu \equiv 1 + 16\pi\kappa/\bar{A}\bar{C}^2$. The free energy must be of course minimized with respect to the parameter (ϕ) of the family of gyroid surfaces.

The phase diagram for $\kappa_1 > 0$ (convex spontaneous curvature) is shown in Figure 7 in variables $\kappa = -\kappa_G/\kappa_2$ and $\bar{\gamma} = \gamma\kappa_2/\kappa_1^2$. Thin lamellae are predicted for $\gamma < 0$; a uniform macroscopic polymer phase is thermodynamically stable for

$$\bar{\gamma} > \bar{\gamma}_t = \frac{1}{2 - \kappa} \tag{44}$$

The spherical and cylindrical mesoglobules and the gyroid bicontinuous phase are predicted at intermediate γ's. Note a wide window of spherical morphology. The curvature C tends to 1 for all morphologies near the multiphase point $\bar{\gamma} = 0.5$, $\kappa = 0$. It corresponds to cylinders of radius $R_{cyl} = L_{ref}$, spheres of radius $R_{sph} = 2L_{ref}$, and primitive gyroid cell of size $L/L_{ref} \approx 7.08$; the fraction of polymer channels in the cell is $2\phi \approx 0.176$.

The inverse morphologies (for $\kappa_1 < 0$) were studied in the same way. Equations 41−43 stay valid also for inverse structures, except that C is now defined in the opposite way ($C > 0$ for convex solvent domains), ϕ must be replaced by $0.5 - \phi$ for inverse gyroid structure, and the free energy for the inverse

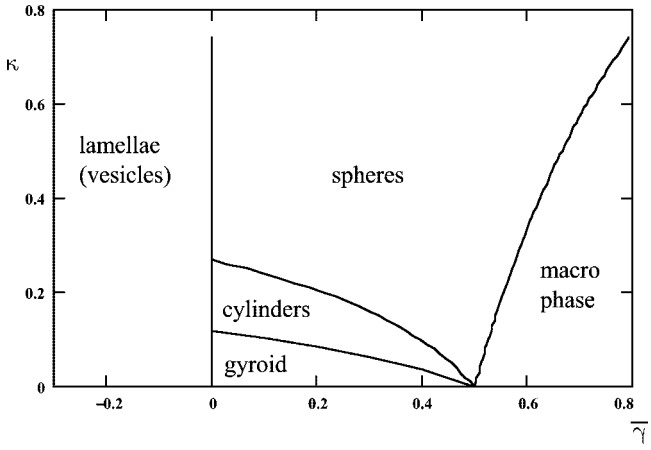

Figure 7. Mesoglobule and bicontinuous morphologies in amphiphilic polymer solutions: The phase diagram for $\kappa_1 > 0$ in variables $\kappa = -\kappa_G/\kappa_2$ (reduced Gaussian modulus) and $\bar{\gamma} = \gamma\kappa_2/\kappa_1^2$ (reduced surface tension).

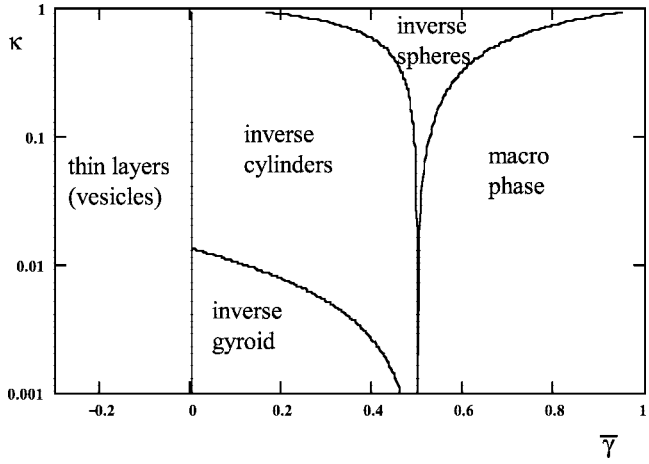

Figure 8. Phase diagram for $\kappa_1 < 0$. The following morphologies are favored as $\bar{\gamma}$ increases for small κ: thin polymer layers, inverse bicontinuous gyroid structure, hexagonally packed inverse cylinders, close-packed inverse spheres, macroscopic polymer phase.

cylindrical and spherical morphologies must be multiplied by an additional factor, $\alpha_{cyl}/2$ and $2\alpha_{sph}/3$, respectively. The phase diagram for $\kappa_1 < 0$ is shown in Figure 8. The inverse morphologies are predicted for $0 \le \bar{\gamma} \le 1/(2 - \kappa)$; the window of inverse cylinders is quite wide; the inverse gyroid region is narrow (it is exaggerated by the log scale used in the plot). The multiphase point $\bar{\gamma} = 0.5$, $\kappa = 0$ is characterized by $C = 1$ as for direct structures. The volume fraction of inverse gyroid (solvent) channels at this point is $2\phi \approx 0.834$; the corresponding gyroid cell size is $L/L_{ref} \approx 0.74$.

6. Discussion and Conclusions

(1) In this paper we analyzed a simple physical model demonstrating the following important property of amphiphilic polymers in poor solvent conditions (when polymer tends to separate from the solvent): by changing the model parameters (like energy ϵ or bond length l), the surface tension γ at the polymer/solvent interface can be decreased down to zero or below; simultaneously, a large volume of the bulk condensed polymer phase remains uniform and stable.[64]

Because of low surface tension, the amphiphilic HP polymers studied in this paper can form stable finite aggregates (mesoglobules) or microdomain structures.

These structures are stabilized by surfactant (amphiphilic) properties of the condensing polymers favoring creation of polymer/solvent interfaces. However, there is an important difference between the amphiphilic polymer structures considered in the present paper and the classical surfactant systems: while the surfactants normally tend to form as much interfacial area as possible, this is not necessarily so for the amphiphilic polymers (as studied here). Note that the most interesting parts of the phase diagrams (see Figures 7 and 8) correspond to the regime of positive (albeit low!) interfacial tension, $\gamma > 0$. Creation of a *plain* interface is not favorable in this regime, although the energy cost is low. In the regime of low positive γ, the amount of interfaces and the characteristic domain size L (the cell size for a bicontinuous structure) are defined by a competition between the *spontaneous* interfacial curvature and the intrinsic structural frustrations associated with the surface bending. In particular, the cell size L is relatively large (as compared to the monomer unit size l) if the spontaneous curvature is weak, as analyzed in the present paper.

In more quantitative terms, the aggregate size and morphology depend on the surface tension γ and on the elastic bending moduli of the polymer/solvent interfaces (κ_1, κ_2, κ_G). The characteristic length scale of the polymer structure is proportional to $L_{ref} = \kappa_2/|\kappa_1|$. Thus, the aggregates/domains are large, $L_{ref} \gg l$, if the spontaneous bending modulus κ_1 is sufficiently small.[65]

(2) The following nondimensional parameters defining the polymer morphology are identified: $\bar{\gamma} = \gamma\kappa_2/\kappa_1^2$ and $\kappa = -\kappa_G/\kappa_2$. The reduced surface tension $\bar{\gamma}$ can take any value depending on the energy and length parameters of HP units; it can also strongly depend on temperature that affects both γ_0 and γ. As for the second parameter, κ (the ratio of Gaussian to mean bending moduli), it shows a much weaker dependence on temperature and other parameters; in all the cases studied $\kappa > 0$ ($\kappa_G < 0$, $\kappa_2 > 0$); typically κ is between 1/3 and 2/3. In this region we predict (for $\kappa_1 > 0$) that the HP polymer forms thin layers (of thickness h comparable with HP unit size l) if γ is negative; a uniform macroscopic polymer phase is formed for large positive γ, and spherical mesoglobules are formed in a relatively wide intermediate regime (positive low γ, see Figure 7).

The last regime is interesting. It provides a framework for explanation of colloidally stable equally sized spherical aggregates observed in solutions of certain thermoresponsive homopolymers.[7,12,26,23−25,54−56] Possibly, the HP polymer model considered here captures the essential features of amphiphilic (homo)polymers. In particular, the finding that typically $\kappa \gtrsim 1/3$ (i.e., $|\kappa_G| \gtrsim \kappa_2/3$) may be quite general. Then, the obtained phase diagram (Figure 7) also provides an explanation why cylindrical mesoglobules are normally not observed in real experiments:[7] cylindrical morphology is predicted for smaller $\kappa < 0.27$. Cylindrical aggregates were obtained in computer modeling study,[15] however, only in the most strong segregation regime (strong attraction of H-subunits that separate from P-subunits and the solvent); the cylinder radius was rather small (of a few HP unit sizes). Possibly, κ_G is small in the strong segregation regime (of high ϵ) studied in ref 15 (note that κ_G decreases with ϵ; see eq 35); hence κ can be low enough in this regime.

(3) The density c_0 in the nearly homogeneous core of a mesoglobule is defined by the energy of attraction between hydrophobic groups (c_0 is considered as a known parameter). We do not assume that this attraction is weak, nor that the core is dilute: on the contrary, the core is assumed to be rather dense. This corresponds to the typical simulation[15] and experimental situations: typical polymer volume fraction inside the aggregates is $\phi_{pol} \sim 0.2-0.7$.[7,12,26,54−56]

(4) Aggregates of amphiphilic macromolecules were studied theoretically in ref 28 for essentially the same HP polymer model

as in the present paper. However, the main regime considered in the previous study was different: they assumed (i) dilute core ($\phi_{pol} \ll 1$) and (ii) thick polymer/solvent interface ($\Delta \gg l$). This regime is not favorable for formation of mesoglobules. In fact, both conditions stated in point (1) above were not fulfilled in the study:[28] On the one hand, the predicted decrease of the surface tension γ due to the presence of soluble P subunits is not strong: γ decreases by less than 10% (for $\epsilon < \epsilon_c$, where ϵ_c is the threshold of the validity of the theory). On the other hand, for larger ϵ ($\epsilon > \epsilon_c$) the uniform aggregate's core becomes unstable with respect to microphase separation (the threshold ϵ_c defines the *spinodal* for the microphase separation, while the *binodal* for this transition corresponds to even lower ϵ).

There is another major difference between the two studies which concerns the key factors controlling the globule shape. In the present paper we show that the shape is defined by the surface free energy (in particular, by the bending energy). In the former study[28] the bending surface energy was not taken into account. Instead, they considered the conformational free energy of a polymer chain confined "inside" a globule. The confinement energy was taken in the form[28]

$$F_{conf} \propto k_B T N \left(\frac{1}{R_1^2} + \frac{1}{R_2^2} + \frac{1}{R_3^2} \right)$$

where $R_{1,2,3}$ are the globule dimensions along the three space coordinates. This expression may be appropriate for an *ideal* polymer chain confined in a box. However, it is totally inapplicable to a polymer chain with *interacting* units forming a large nearly *uniform* globule (except a relatively thin interfacial layer). In this case the conformational energy comes entirely from the interfacial layer (this free energy is already included in the surface energy); there is no conformational contribution of the globule core since the core is *uniform*.

(5) Let us turn to the temperature dependence of the size of spherical mesoglobules. The predicted globule radius is (see section 5.6, eq 42)

$$R \simeq \frac{3(2\kappa_2 + \kappa_G)}{2\kappa_1 + \sqrt{4\kappa_1^2 - 3\gamma(2\kappa_2 + \kappa_G)}} \tag{45}$$

The most important parameters here are κ_1 and γ: both parameters must be positive and small in the region of interest (where R is large); hence they must be sensitive to the solvent quality. It is natural to assume that γ increases as solvent quality decreases (due to a T variation, either a decrease of T or an increase of T in the case of thermosensitive polymers like PNIPAM near a lower critical solution temperature, LCST). One may expect that κ_1 shows a similar behavior provided that $\kappa_1 > 0$ initially (see eqs 34; note that concentration $\psi_0 \propto c_0$ increases as the solvent becomes poorer). Neglecting a variation of $2\kappa_2 + \kappa_G$ and assuming a linear relationship between κ_1 and γ

$$2\kappa_1 \simeq A\gamma + B, \quad A > 0 \tag{46}$$

lead to

$$R \simeq \frac{\text{const}}{1 + \beta\Gamma + \sqrt{(1 + \beta\Gamma)^2 - \Gamma}}$$

where $\Gamma \equiv 3(2\kappa_2 + \kappa_G)\gamma/B^2 \propto \gamma$ is the measure of solvent quality (Γ depends on temperature), and

$$\beta = AB/[3(2\kappa_2 + \kappa_G)] \simeq \text{const} \tag{47}$$

The spherical morphology is stable if $\Gamma > 0$ and

$$(1 + \beta\Gamma)^2 > \frac{4}{3}\Gamma \tag{48}$$

(this condition is equivalent to $\bar{\gamma} < 1/(2 - \kappa)$; see eqs 42).

The temperature dependence of R crucially depends on the parameter β. If $1/4 < \beta < 1/3$, then R decreases with Γ (i.e., as solvent quality decreases) up to $\Gamma = \Gamma_{t1}$; a macroscopic polymer phase is stable for higher Γ ($\Gamma_{t1} < \Gamma < \Gamma_{t2}$), and a re-entrant spherical morphology emerges for $\Gamma > \Gamma_{t2}$; R is also decreasing with Γ in the re-entrant regime. The regime of macroscopic phase separation shrinks as β tends to 1/3. For $0 < \beta < 1/4$, R increases with Γ below Γ_{t1}; otherwise its behavior is similar. This sort of behavior of R (an increase with the depth of temperature quench into the phase separation region) was observed for PNIPAM (high molecular weight, $M \approx 2 \times 10^6$, low concentration, $c \approx 10^{-4}$ g/cm^3) in a rather narrow range of quench temperatures ($T = 32.8-33.8$ °C) above the LCST (≈31 °C).[24] A similar behavior (increase of R on heating) was also found for lower molecular weight PNIPAM ($M \approx 5 \times 10^4$) at the same concentration and in about the same temperature range ($T = 31-33$ °C).[54] For $\beta > 1/3$ the mesoglobule radius R is decreasing with Γ all the way, and the macroscopic phase separation is avoided. Such behavior of the aggregate size (decrease of R as the thermodynamic quality of the solvent decreases) was often observed for PNIPAM or PVME solutions at 3−10 °C above the LCST.[7,55] On the other hand, the first scenario (for $1/4 < \beta < 1/3$) allows to rationalize a more interesting behavior of the mesoglobule size that was sometimes observed in solutions of amphiphilic polymers: a decrease of R followed by its sharp increase as solvent quality becomes more poor[14,15] (the increase is in turn followed by a weak decrease of R). It may be reasonable to associate the sharp increase of the globule size with the transition from finite globules to infinite macroscopic condensed polymer phase. Above the transition (i.e., for $\Gamma > \Gamma_{t1}$) the globules start to coalesce; this process however significantly slows down as the polymer droplets grow: the droplet fusion is opposed by an energy barrier due to a repulsion of hydrophilic P-layers surrounding the droplets. This barrier increases with the droplet size, so the droplet growth may essentially stop at some size threshold. The resulting behavior may look like a sharp increase in size of polymer aggregates as Γ rises beyond Γ_{t1}. A weak decrease of R upon the transition may be simply due to compaction of the aggregates in poor solvent conditions (an increase of their density at kinetically fixed aggregation number).

(6) The number of HP units in a mesoglobule is

$$N_g = c_0 V_g$$

where $V_g = 4\pi R^3/3$ is the globule volume and c_0 is concentration of the units (note that $c_0 = \psi_0$ for amphiphilic *homo*polymers considered here). N_g is large since R is large ($R \gg a_H$). If the polymerization degree N is comparable to N_g, significant quantization effects are expected. (The quantization affects both the globule size and the region of thermodynamic stability of spherical morphology: spherical aggregates can be somewhat destabilized in favor of either cylinders or macroscopic polymer phase.) This regime ($N \sim N_g$) is not further considered here. The theoretical treatment of spherical aggregates provided in section 5 is applicable for $N \ll N_g$. This case corresponds to mesoglobules with large aggregation number $m = N_g/N \gg 1$; this regime is typical in experiments on amphiphilic polymers.[7,13,14,24,55,56] The predicted radius of mesoglobules, R, nearly does not depend on polymer molecular mass (i.e., on N) in this regime, in qualitative agreement with experiments.[7]

In the opposite case, $N \gg N_g$, each polymer chain forms many optimum globules (beads). The following structures are then possible (see Figure 9): a linear sequence (garland) of beads, a branched structure of beads, and a compact aggregate of beads (condensed garland of beads). In all the cases the beads are

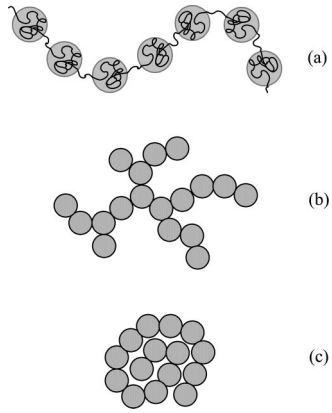

Figure 9. (a) A linear sequence (garland) of globules connected by short stretched chain fragments (bridges). (b) A branched structure of globules. (c) A compact aggregate of globules (condensed garland).

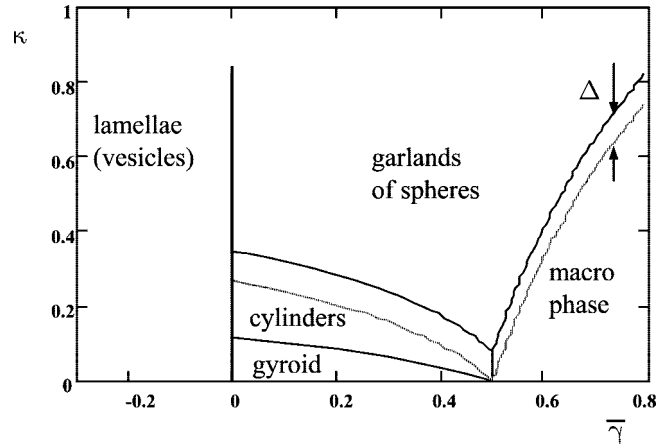

Figure 10. Phase diagram for very long polymer chains, $N \gg N_g$ (and for $\kappa_1 > 0$). Linear garlands of spherical globules instead of isolated mesoglobules are formed in this case. $\Delta = E_b/(4\pi\kappa_2)$, where E_b is the bridge energy. Dashed lines are copied from the diagram of Figure 7; they correspond to $E_b = 0$.

connected by uncollapsed (stretched) main-chain fragments (bridges). Globules connected by necks (see Figure 4f) are never favorable since such structure always has higher free energy than a cylindrical aggregate (see Appendix E). Aggregation of polymer beads was analyzed in ref 62 for polysoaps with soluble backbone. The driving force for aggregation is the bridging attraction[59] of entropic origin. However, this effect is suppressed for the model (with hydrophobic main chain) considered in the present paper. The reason is related to the high enthalpic cost E_b of a bridge: each bridging fragment necessarily involves many unfavorable interactions of the hydrophobic main chain with solvent molecules (note that the typical distance between the beads is $\gtrsim 2l$, $l \gg a_H$; hence a bridging fragment consists of many H-subunits, and $E_b \sim k_BTl/a_H \gg k_BT$). Therefore, the system must tend to minimize the number of bridges; i.e., a *linear* sequence of beads must be favored. Such necklace structure was predicted[63] for graft copolymers in the polysurfactant regime, when the bead size is comparable to the copolymer block size.

The garland structures of "amphiphilic" beads are somewhat reminiscent of well-known polyelectrolyte necklace structures.[66] However, the physical reason for formation of mesoscopic beads is entirely different in the latter case: formation of large PE pearls is dictated, in particular, by *long-range* Coulomb interactions, while all interactions are *short-range* in the case of model amphiphilic polymers considered in the present paper.

The bridges affect both the size and the window of stability of the spherical morphology. For long garlands ($N \gg N_g$) there is one bridge per globule, so the free energy per unit volume increases by E_b/V_g. This change is equivalent to a renormalization $\kappa_G \rightarrow \kappa_G + E_b/4\pi$, $\kappa \rightarrow \kappa^* = \kappa - E_b/4\pi\kappa_2$. The globule size increases:

$$R \simeq \frac{3\left(2\kappa_2 + \kappa_G + \frac{E_b}{4\pi}\right)}{2\kappa_1 + \sqrt{4\kappa_1^2 - 3\gamma\left(2\kappa_2 + \kappa_G + \frac{E_b}{4\pi}\right)}}$$

and the region of stability of the spherical structure somewhat shrinks as a result (see Figure 10).

(7) Experimental studies[9−11] of globule−coil transitions in high molecular weight PNIPAM and poly(*N*-isopropylmethacrylamide) indicate that this transition is not an "all-or-none" process: rather, homopolymer globules consist of several cooperative units ("melting domains") whose number n_d is proportional to the molecular weight M of the polymer (n_d is ranging from 1 to 120 for $M \sim 10^4-7 \times 10^6$). Possibly, at the globule to coil transition point these polymers form garlands of condensed beads connected by short coil fragments (see Figure 9).

(8) There are many reports that aqueous PNIPAM solutions can phase separate forming colloidally stable polymer particles.[12,23−26,55,56] The PNIPAM particles sized in the 50−200 nm range contained either single[12] or several polymer chains (up to ~500[56]). It was suggested that PNIPAM aggregates are stabilized by repulsion of charged sulfate groups attached to PNIPAM chain ends during initiation of the polymerization reaction.[56] While this stabilization mechanism may be at work in some cases (e.g., for large aggregates of more than ~50 chains), it certainly is not important for single-chain PNIPAM globules: Even with no electrostatic screening (zero ionic strength), the energy of repulsion of two sulfate groups is

$$U \sim \frac{l_B z^2}{r} k_BT \sim 0.03 k_BT$$

i.e., it is 10^3 lower than the typical repulsion energy ($\sim 30k_BT$) required for the stabilization. Here $l_B \simeq 0.7$ nm is the Bjerrum length in water, $r \sim 100$ nm is the distance between the charges ($r = 2D$, where $D \sim 50$ nm is the globule diameter[12]), and $ze = 2e$ is the charge per group. In addition, while adding a salt results in an increase of the particle size D, the typical ionic strength producing a significant effect (~0.01 M)[56] corresponds to the Debye length $r_D \sim 3$ nm that does not match either the particle size ($D \sim 100$ nm) or the interparticle distance (~2 μm). It is likely that electrostatic effects are not important for other nonionic homopolymers, PVCL, PVME, that, however, also forms stable colloids in aqueous solutions.[13] Also, the more recently synthesized PNIPAM has no charged ends.[7,55] Therefore, electrostatic repulsion between polymer mesoglobules cannot, in the general case, account for their stability.

(9) Stability of mesoglobules. In this paper we investigated the *equilibrium* structure in solutions of amphiphilic polymers. It is likely, however, that *kinetic* effects can be important in practice for the mesoglobule formation/transformation. These effects are discussed briefly below.

Consider a system of mesoglobules which is not at the thermodynamic equilibrium: either the aggregate size R deviates from the optimum size R_{eq}, or the equilibrium morphology is different (for example, the homogeneous macroscopic polymer phase is more favorable than globules). There are two classical mechanisms by which the system can evolve to the true equilibrium: by fusion/fission of globules (fusion for $R < R_{eq}$, fission for $R > R_{eq}$) and by diffusion coalescence (Ostwald

ripening). For amphiphilic polymer aggregates the fusion/fission processes can be significantly slowed down by high activation energy barriers. The barrier for fusion is due to repulsion of soluble P-subunits forming the surface layers of the globules; this barrier is increasing with globule size. The energy penalty for fission is due to the surface energy increase necessitated by the process involving the globule deformation. This penalty is proportional to κ_2. For example, it amounts to roughly $11\kappa_2$ for $\bar{\gamma} = 1/2$ and $R \gg R_{eq}$ (this estimate can be obtained using the results of ref 57). Apart from the activation barriers, the fusion/fission processes can be affected by the quantization effects. Consider, for example, a system of spherical mesoglobules ($\kappa_1 > 0$) near the threshold for macroscopic phase separation, i.e., at γ just below $\gamma_t = (\kappa_1^2/\kappa_2)[1/(2-\kappa)]$ (see eq 44). It is assumed that the system has reached the equilibrium state at this γ, so the mesoglobules have the equilibrium size $R_{eq} \simeq (2-\kappa)\kappa_2/\kappa_1$ (see eq 45). Macroscopic polymer droplets become more favorable than the R_{eq}-mesoglobules as soon as the surface tension increases above γ_t. Nevertheless, fusion of two R_{eq}-globules is not favorable just above γ_t: an additional increase of γ (by a factor of α_2) is required to turn on the fusion process (for $\gamma < \alpha_2\gamma_t$ the initial free energy of two metastable globules is lower than the free energy of the larger globule formed upon their fusion). This effect is more pronounced if κ_1 increases in parallel with γ as discussed in point (5) (see eq 46). The factor α_2 increases as the parameter β defined in eq 47 is increased: $\alpha_2 \approx 1.5$ for $\beta = 0.2$, $\alpha_2 \approx 2.6$ for $\beta = 0.25$. Fusion of two R_{eq} globules is never favorable if $\beta > 0.264$ (higher-order fusion processes, for example, triple collisions, are then required for the aggregate growth to proceed).

(10) Let us turn to the second mechanism: diffusion coalescence (Lifshitz−Slyozov coalescence mechanism of Ostwald ripening). The classical Lifshitz−Slyozov coalescence process[52] involves evaporation of molecules from smaller droplets, their diffusion, and condensation onto larger droplets. Thus, smaller droplets disappear and larger droplets grow. The driving force for this process is the droplet surface tension. In the case of amphiphilic polymer mesoglobules a polymer chain can also detach from one mesoglobule, diffuse, and then associate with another mesoglobule (it is the regime of many chains per aggregate, $m \gg 1$, that is considered here). This process is slow since the concentration of polymer chains in the solvent matrix is low, but still it is going on. The point is, however, that (if the droplet size is not too far from equilibrium) the coalescence process results not in a growth of larger droplets at the expense of small ones but, on the contrary, in the opposite tendency: the mesoglobules approach the same size (both from above and from below); i.e., the diffusion coalescence keeps the system of droplets monodisperse. (This statement is in agreement with experiments: a very narrow size distribution of aggregates of thermosensitive amphiphilic homopolymers was reported.[7]) This is obviously true if the globule size R nearly corresponds to thermodynamic equilibrium ($R = R_{eq}$) but is also true for a wide range of nonequilibrium sizes.

To see this, let us analyze the stability of a system of mesoglobules. Note that in the absence of fusion/fission/nucleation processes the total number of mesoglobules, $\mathcal{N}$, is fixed. The total volume $\mathcal{V}$ of the globules is fixed as well. The following physical analogy is then useful: the free energy of a polydisperse system of noninteracting mesoglobules can be formally mapped to that of a nonuniform "real gas". The total volume occupied by the gas is $\mathcal{V}$, and the number of gas particles is $\mathcal{N}$. The local gas concentration is then analogous to the inverse volume of a mesoglobule $((4\pi/3)R^3)^{-1}$. For simplicity, we omit the numerical coefficient and define the "concentration" variable as just $y = R^{-3}$. The density of the gas free energy is analogous to the mesoglobule free energy per unit volume F. The classical theory of first-order phase transitions, as applied to the function $F(y)$, then says that a monodisperse system of mesoglobules (corresponding to a uniform state of the "real gas") is stable if $\partial^2 F/\partial y^2 > 0$. For spherical aggregates (only the surface energy is considered, as before)

$$F = 3[\gamma y^{1/3} - 2\kappa_1 y^{2/3} + (2\kappa_2 + \kappa_G)y]$$

The stability condition then becomes ($\kappa_1 > 0$ is assumed):

$$R < R^* = \frac{2\kappa_1}{\gamma}$$

Let us apply this result to the formation of macroscopic polymer phase from spherical mesoglobules. At the equilibrium transition line (the rightmost line in the phase diagram, Figure 7)

$$\gamma_t = \frac{{\kappa_1}^2}{2\kappa_2 + \kappa_G}, \quad R_{eq} = \frac{2\kappa_2 + \kappa_G}{\kappa_1}, \quad R^* = 2R_{eq}$$

Let us assume that at $\gamma = \gamma_t$ the mesoglobules have the equilibrium size $R = R_{eq}$. The stability criterion then says that the monodisperse system of mesoglobules is (locally) stable not only at $\gamma = \gamma_t$, but also above γ_t. If $\kappa_1 = \text{const}$, then γ must be significantly increased above $\gamma^* \simeq 2\gamma_t$ to induce a spinodal-like destabilization of the system (here we neglect a variation of concentration in the condensed polymer phase, so it is assumed that $R \simeq R_{eq}$ for $\gamma_t < \gamma < \gamma^*$). If κ_1 also increases with γ, then the critical γ^* increases further (γ^*/γ_t is a function of the parameter β, see point (5): $\gamma^*/\gamma_t = 3$ for $\beta = 0.25$; γ^*/γ_t tends to infinity, i.e., the instability region disappears, for $\beta > 1/3$).

(11) Now, let us turn to the instability regime $\gamma > \gamma^*$. In this case the larger mesoglobules start to grow, while the smaller ones decrease in size. However, the small globules do not "evaporate" completely: rather, their size decreases by a factor of 2 (at $\gamma = \gamma^*$). In fact, for $\gamma > \gamma^*$ the system of mesoglobules "phase separates" in two populations: one (or a few) macroscopically large aggregates and many globules of size

$$R_m = \frac{\kappa_1}{\gamma} \tag{49}$$

This "phase separation" (and the above result for R_m) can be obtained applying the classical tangential line method to the free energy function $F(y)$. Note that R_m is exactly 1/2 of the critical R^*. This means that just above γ^* the total volume of condensed polymer is distributed in the following way: 1/8 of the volume is in the form of R_m mesoglobules as the radius of finite aggregates decreases twice (the number of mesoglobules does not change: a few macroscopic aggregates does not count) and 7/8 of the volume belongs to the macroscopic phase. The R_m mesoglobules are in a metastable equilibrium with the macroscopic phase. As γ increases further, their size follows eq 49: in terms of the reduced surface tension Γ defined in point (5) the size decreases as $R_m \propto 1/\Gamma + \beta$.

(12) We are now in a position to discuss the dependence of the polymer droplet size on the temperature quench rate, on the quench depth, and on polymer concentration. The equilibrium size temperature dependence was already considered (see point (5)). There are indications, however, that the size of mesoglobules can be kinetically defined (for example, the size of PNIPAM aggregates depends on heating rate[7,24]). The tentative kinetic scenario is outlined below.

Suppose a dilute solution of high-molecular-weight amphiphilic polymer (e.g., PNIPAM) is quenched into the phase separation region. The separation process then starts with a collapse of individual polymer chains, i.e., globule formation (spinodal decomposition mechanism is totally irrelevant in the dilute regime where polymer coils are not overlapping: note

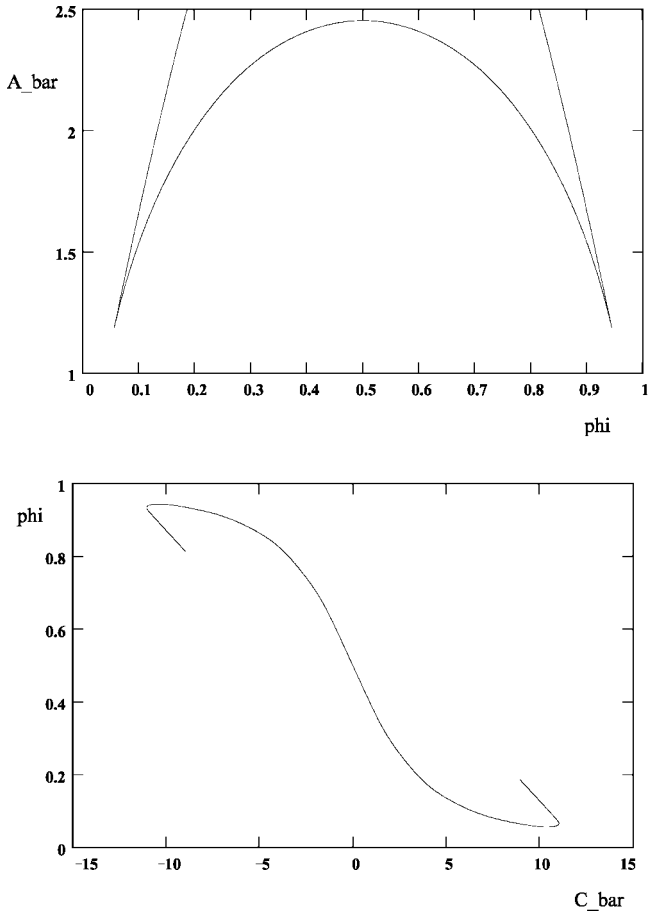

Figure 11. Relationships between the reduced surface area $\bar{A}$ per primitive cell for gyroid G-family of CMC surfaces, volume fraction ϕ to one side of the surface, and the (doubled) reduced mean curvature, $\bar{C}$. (By definition the Euler−Poincare characteristic of the primitive cell is $n_E = -4$; volume per cell is L^3; $\bar{A} = A/L^2$, $\bar{C} = CL$.)

that the typical polymer concentration is very low indeed, $c \sim 10^{-4}$ g/cm^3). The primary globules then collide and aggregate in larger particles. As long as the particle size is not too large, $R < R^*$, their size distribution is kept nearly monodisperse by the diffusion−coalescence mechanism described above. As the total volume of all the polymer particles is nearly constant, the particle size is simply proportional to the inverse cubic root of their number. Each fusion event reduces the number, thus increasing the size R. The fusion rate, however, decreases dramatically with R due to the slowing down effect of repulsion of hydrophilic surface layers (the corresponding activation energy becomes higher for larger R). Therefore, the growth saturates at some R_{app}. The saturated size R_{app} can be smaller than R^*. (The size R_{app} is controlled by the activation effects of surface layer repulsion if fusion of two polymer particles is thermodynamically favorable, which is the case for high enough γ or low enough R_{app}. Otherwise, the size R_{app} is determined by the thermodynamic effect considered in the point (9): the fusion must significantly slow down as soon as the free energy change on fusion of two particles becomes positive.) The following tendencies are implied by this picture:

(i) As the frequency of particle collisions increase with their concentration, we expect that R_{app} also increases with the average polymer concentration c. This prediction is in qualitative agreement with experimental data on PNIPAM.[7,24,56] If the system is diluted after mesoglobule formation at some concentration, collision and fusion rates drop; hence the number of mesoglobules and their size does not change on dilution, as observed for PNIPAM solutions.[7,24]

(ii) For PNIPAM solutions, as T rises above the LCST, the particle density increases, and so does the density of the hydrophilic surface layers. Therefore, the repulsion of two such surface layers can become stronger with the depth of T-quench; hence, the fusion rate decreases at higher T. This feature explains why the particle size can decrease with T[55] (lower fusion rate implies larger number of smaller mesoglobules), but also why R decreases with heating rate[7,24] (higher heating rate means shorter time spend in the favorable for fusion low-T regime).

A further consideration of the fusion/fission processes is outside the scope of the present paper.

(13) Two kinds of nearly monodisperse spherical mesoglobules are predicted for $\kappa_1 > 0$: (i) equilibrium (thermodynamically stable) particles of size R_{eq} (see the region of spheres in the diagram of Figure 7) and (ii) *metastable* mesoglobules (of size R_m). The equilibrium mesoglobules are expected if both the surface tension γ and the spontaneous bending modulus κ_1 are low. The metastable aggregates coexist with the macroscopic polymer phase. They can be stable in a wider regime where macroscopic phase is thermodynamically favorable, but also where the macrophase is metastable (i.e., where smaller equilibrium droplets are favored thermodynamically). The sizes R_{eq} and R_m are entirely different. The size R_{eq} is essentially inversely proportional to κ_1 (see eq 45); it is large if κ_1 is low. The size R_m is inversely proportional to the surface tension γ, and it *increases* with κ_1 (see eq 49). Thus, low surface tension is the essential requirement (apart from $\kappa_1 > 0$) for the existence of large metastable droplets.

Acknowledgment. E.A.M. acknowledges support from Université Louis Pasteur.

Appendix A. Bending Energy of Spherical Surface

Consider a spherical globule of core radius $R \gg l$. Its surface energy can be written in analogy with eq 8 (the γ_0 contribution is omitted for simplicity):

$$f_s = -\psi_0 \int_0^l \ln\left(1 + \frac{\Omega}{4\pi}(e^{\epsilon} - 1)\right)(1 - x/R)^2\, dx \quad \text{(A1)}$$

Here and below (in Appendices A−C) we consider l as the length unit. The factor $(1 - x/R)^2$ defines the relative area of the spherical surface of radius $r = R - x$, and $\Omega = \Omega(x)$ is the solid angle covered by an HP unit with H-group fixed at the distance x from the core/solvent interface (at $r_H = R - x$) and with P-group anywhere outside the core ($r_P > R$). $\Omega(x)$ is defined by the simple spherical geometry; upon expansion as a series in $1/R$, it becomes (in the quadratic approximation which is sufficient for our purposes)

$$\Omega(x) \simeq 2\pi(1 - x)\left[1 + \frac{1}{2R}(1 + x) + \frac{1}{2R^2}x(1 + x)\right] \quad \text{(A2)}$$

After a transformation eq A1 reads

$$f_s = \psi_0 \int_0^1 \frac{x(1 - x/R + x^2/3R^2)}{\Omega + 2\pi(\Lambda - 1)} \frac{d\Omega}{dx}\, dx$$

where

$$\Lambda = \frac{e^{\epsilon} + 1}{e^{\epsilon} - 1} \quad \text{(A3)}$$

Expanding f_s for small $1/R$ and taking the resultant integrals, we obtain

$$f_s \simeq \gamma_P - \psi_0\frac{1}{2R}\left[3\Lambda + \frac{3}{2} - (3\Lambda^2 - 1)\ln\frac{\Lambda}{\Lambda - 1}\right] - \psi_0\frac{1}{R^2}\left[\frac{1}{8\Lambda} + \frac{5}{9} - \frac{2}{3}\Lambda - \frac{4}{3}\Lambda^2 + \Lambda\left(\frac{4}{3}\Lambda^2 - 1\right)\ln\frac{\Lambda}{\Lambda - 1}\right]$$

where γ_P is defined in eq 9.

Appendix B. Cylindrical Surface Energy

Now let us turn to the cylindrical surface with curvature $C = 1/R$. The surface energy per unit area is (compare with eq A1)

$$f_s = -\psi_0\int_0^l \ln\left(1 + \frac{\Omega}{4\pi}(e^{\epsilon} - 1)\right)(1 - Cx)\,dx \qquad (B1)$$

where $\Omega = \Omega(x)$ has the same meaning as before. Its calculation is outlined below.

Consider a point H inside the cylinder at the distance x from its surface; the HP vector orientation is defined by spherical angles θ (the polar angle between HP and the cylindrical axis) and φ (the azimuthal angle between the projection of HP onto the cylinder cross section and its radius pointing to H). The condition that P is outside the cylinder reads

$$(R - x)^2 + (l\sin\theta)^2 + 2l(R - x)\sin\theta\cos\varphi > R^2 \qquad (B2)$$

The corresponding body angle is

$$\Omega(x) = \int \sin\theta\,d\theta\,d\varphi$$

where the integration region is defined by the condition (B2). Integrations over φ and then—by parts—over θ yield

$$\Omega = 2\int_0^1 \frac{\sqrt{1 - y}(\alpha/y - \beta)}{\sqrt{y - (\alpha + \beta y)^2}}\,dy$$

where $\alpha = [(2R - x)x]/[2(R - x)]$, $\beta = -1/[2(R - x)]$, and $y = \sin^2\theta$. Expanding Ω for small $C = 1/R$, we get

$$\Omega \simeq 2\pi(1 - x)\left[1 + \frac{C}{4}(1 + x) + \frac{3}{16}C^2x(1 + x)\right] \qquad (B3)$$

Substituting (B3) in (B1) after some algebra, we get

$$f_s \simeq \gamma_P - \psi_0\frac{C}{4}\left[3\Lambda + \frac{3}{2} - (3\Lambda^2 - 1)\ln\frac{\Lambda}{\Lambda - 1}\right] - \frac{\psi_0C^2}{16}\left[\frac{1}{2\Lambda} + 2 - \frac{3}{2}\Lambda - 3\Lambda^2 + 3\Lambda(\Lambda^2 - 1)\ln\frac{\Lambda}{\Lambda - 1}\right]$$

where γ_P is defined in eq 9 and Λ in eq A3.

Appendix C. Interaction Energy

1. Plain Surface. Consider a globule (polymer phase) with plain core/solvent interface at $x = 0$. To calculate $\Delta\mathcal{F}_B$, we have to find the concentration profile $c_P(x)$ *outside* the core:

$$c_P(x) = \int_0^{1-x} c(x', x)\,dx' \qquad (C1)$$

where $c(x', x)\,dx'$ is the partial concentration of P-subunits (outside the core at the distance x from its surface) connected to H-groups located inside the core in the layer of thickness dx' at the distance x' from the surface (the HP bond length l is chosen as the length unit as before). Obviously

$$x' + x = \cos\theta \qquad (C2)$$

where θ is the angle between HP bond and the normal to the surface. For $B = B' = 0$, $\epsilon = 0$, the HP bond orientations are distributed isotropically (for any given position of the modified main-chain H-unit), and the H-units are uniformly distributed inside the core, so the unperturbed partial concentration can be found in a simple way:

$$c(x', x)\,dx = \psi_0\frac{d\Omega}{4\pi} = \frac{1}{2}\psi_0\,dx \qquad (C3)$$

where $d\Omega$ is the solid angle covered by HP spacers with H-end at x' inside the core and P-end in the layer $(x, x + dx)$ outside. Hence, for $0 < x < 1$

$$c_P(x) = \frac{\psi_0}{2}(1 - x)$$

Thus, the free energy per unit area $\Delta f_B = \Delta\mathcal{F}_B/\mathcal{A}$ is

$$\Delta f_B \simeq \frac{B}{2}\int c_P(x)^2\,dx = \frac{B\psi_0^2}{24}$$

The inner contribution $\Delta f_{B'}$ can be easily found noting that the HP spacers of the initial globule (with the core to the left of the surface $x = 0$) and of the ghost inverse globule (with the core to the right of the surface), jointly, are characterized by a uniform and isotropic position/orientation distribution in the whole space. The result is $\Delta f_{B'} = B'\psi_0^2/24$.

2. Spherical Surface. For a spherical globule of radius R, the simple relations (C2) and (C3) are replaced by

$$(R + x)^2 = 1 + (R - x')^2 + 2(R - x')\cos\theta \qquad (C4)$$

$$(R + x)^2c(x', x)\,dx = (R - x')^2\psi_0\frac{d\Omega}{4\pi} \qquad (C5)$$

Here θ is the angle between HP and the radius pointing to the H-group, and x, x' have the same meaning (the distances of P- and H-subunits to the globule surface).

Using eqs C4, C5, C1, we find

$$c_P(x) = \frac{\psi_0}{2}\frac{1 - x}{1 + x/R}\left[1 - \frac{1}{2R}(1 - x)\right]$$

Thus, we get

$$\Delta f_B = \frac{B}{2}\int c_P(x)^2(1 + x/R)^2\,dx \simeq \frac{B\psi_0^2}{8}\left(\frac{1}{3} - \frac{1}{4R} + \frac{1}{20R^2}\right) \qquad (C6)$$

The inner energy is

$$\Delta f_{B'} \simeq \frac{B'\psi_0^2}{8}\left(\frac{1}{3} + \frac{1}{4R} + \frac{1}{20R^2}\right) \qquad (C7)$$

3. Cylindrical Surface of Radius $R = 1/C$. In the cylindrical case eq C2 is generalized as

$$(R + x)^2 = \sin^2\theta + (R - x')^2 + 2\sin\theta(R - x')\cos\varphi$$

which is equivalent to

$$\cos\varphi = \alpha/\sin\theta + \beta\sin\theta$$

where

$$\alpha = \frac{x' + x}{2}\frac{2 + Cx - Cx'}{1 - Cx'}, \quad \beta = -\frac{C}{2(1 - Cx')}$$

and the angles θ and φ are defined just before eq B2.

Equation C3 is now replaced by

$$(1 + Cx)c(x', x)\,dx = \psi_0(1 - Cx')\frac{d\Omega}{4\pi} \qquad (C8)$$

where

$$d\Omega = d(\int \sin\theta\, d\theta\, d\varphi) = 2I\, d\alpha$$

$$I \equiv 2\int \frac{d\theta}{|\sin\varphi|} = 2\int_{(x'+x)^2}^{1} \frac{dt}{\sqrt{1-t}\sqrt{t-(\alpha+\beta t)^2}}$$

and $d\alpha = (1 + Cx)/(1 - Cx')\, dx$. Taking the last integral, we find

$$I/\pi \simeq 1 - \frac{C}{2}(x'+x) + \frac{C^2}{4}\left[\frac{1}{4} + \frac{9}{4}(x'+x)^2 - (x'+x)(3x'+x)\right]$$

On using eqs. (C1), (C8), we obtain:

$$c_P(x) \simeq \frac{\psi_0}{2}(1-x)\left[1 - \frac{C}{4}(1+x) + \frac{3C^2}{16}x(1+x)\right]$$

Finally

$$\Delta f_B = \frac{B}{2}\int_0^1 c_P(x)^2(1+Cx)\, dx \simeq \frac{B\psi_0^2}{8}\left(\frac{1}{3} - \frac{C}{8} + \frac{C^2}{80}\right) \quad \text{(C9)}$$

The inner contribution is

$$\Delta f_{B'} \simeq \frac{B'\psi_0^2}{8}\left(\frac{1}{3} + \frac{C}{8} + \frac{C^2}{80}\right) \quad \text{(C10)}$$

Appendix D. Microphase Separation in the Core

Here we briefly consider the conditions of stability of a homogeneous globule core with respect to microdomain superstructure formation.

1. Spinodal. Using the standard approach,[60] we write the free energy increment $\delta\mathcal{F}$ due to a weak inhomogeneity $\delta c(x) \equiv \delta c_P(x)$ as

$$\delta\mathcal{F} \simeq \frac{1}{2}\sum_q \Gamma(q)\delta c_q \delta c_{-q}$$

where δc_q is the Fourier image of $\delta c(x)$ (here x is position vector, q is wave-vector) and

$$\Gamma(q) = \Gamma_0(q) - |B'|$$

is the vertex function (recall that $B' < 0$). Here $\Gamma_0(q) = 1/S_0(q)$, where $S_0(q) = \langle \delta c_q \delta c_{-q}\rangle_0$ is the correlation function of P-concentration fluctuations in the ideal HP system (P-groups are attached to homogeneously distributed H-points by freely rotating rigid rods of length l):

$$S_0(q) = \psi_0\left(1 - \frac{\sin^2(ql)}{(ql)^2}\right)$$

The spinodal defined by the condition $\min_q \Gamma(q) = 0$ corresponds to

$$|B'| = |B'|_s = 1/\psi_0 \quad \text{(D1)}$$

(Note that a homogeneous distribution of H-groups was assumed in this derivation. Generally, a fluctuation δc_P induces an inhomogeneity δc_H of the concentration profile of H-groups. However, this δc_H is very weak, and its effect is negligible since the volume fraction of P-groups is small, $p \equiv v_P/nv_H \ll 1$.)

2. Binodal. Attraction of P-groups (quantified by $|B'|$) can lead to their aggregation in the core. The binodal corresponds to the threshold $|B'|_b$ beyond which the formation of P-aggregates is favorable. An analysis shows that the critical P-aggregates are large (consist of $m \gg 1$ P-groups) if

$$l^2\psi_0 v_P^{1/3} \gg 1 \quad \text{(D2)}$$

This condition is similar to the condition (17) adopted in this paper. The condition (D2) ensures that $1 \ll m \ll l^3\psi_0^{3/2}v_P^{1/2}$ and that the free energy $\mathcal{F}_a$ of an aggregate includes two main contributions:

$$\mathcal{F}_a \simeq \mathcal{F}_{id} + \mathcal{F}_{int}$$

Here $\mathcal{F}_{id} = V_a(c_P \ln(c_P/\psi_0) + \psi_0 - c_P)$ is the excess ideal-gas free energy (compare with eq 3.7 of ref 53), V_a is the volume of an aggregate, $c_P = m/V_a$ is P-concentration inside the aggregate, and $F_{int} = V_a(B'/2)(c_P - \psi_0)^2$ is the excess interaction free energy. The binodal condition is $\min_{c_P>\psi_0} \mathcal{F}_a/m = 0$; it leads to the following critical parameters: $c_P = c_{max} = 1/v_P$, $|B'|_b \simeq 2\ln(1/e\psi_0 v_P)$. The regime of homogeneous core is therefore defined by

$$|B'| < 2\ln\frac{1}{e\psi_0 v_P} \quad \text{(D3)}$$

Appendix E. Modulated Cylinder

The axially symmetric modulated cylindrical surface is defined by the constant mean curvature equation:

$$\frac{1}{\sqrt{1+r'^2}}\left(\frac{1}{r} - \frac{r''}{1+r'^2}\right) = C = \text{const} \quad \text{(E1)}$$

where $r = r(z)$, $r' = dr/dz$ (r, z are cylindrical coordinates; r is distance to the axis, z is distance along the axis). For simplicity, we set $C = 1$ below in this section. Equation E1 can be integrated (the first integral can be obtained using, for example, the extremal property of the surface: it locally minimizes the surface area for a fixed volume inside) yielding

$$1 - \frac{2r}{\sqrt{1+r'^2}} + r^2 = \delta^2$$

where $\delta = \text{const}$, $0 \le \delta \le 1$. $\delta = 0$ corresponds to a cylinder of radius 1. $\delta = 1$ corresponds to a sequence of spheres of radius 2. A modulated cylinder emerges between these two limits. The half-period of the structure is

$$H = \int_{r_-}^{r_+} \frac{1 - \delta^2 + r^2}{\sqrt{(r^2 - r_-^2)(r_+^2 - r^2)}}\, dr$$

where $r_- = 1 - \delta$, $r_+ = 1 + \delta$. The surface area $\bar{A}$ and the volume $\bar{V}$ inside the surface per half-period are

$$\bar{A} = 4\pi\int_{r_-}^{r_+} \frac{r^2\, dr}{\sqrt{(r^2 - r_-^2)(r_+^2 - r^2)}};$$

$$\bar{V} = \pi\int_{r_-}^{r_+} \frac{r^2(1 - \delta^2 + r^2)\, dr}{\sqrt{(r^2 - r_-^2)(r_+^2 - r^2)}}$$

Note the following useful relations:

$$2\bar{A} = 3\bar{V} + \pi(1-\delta^2)H$$

$$d\bar{A} = d\bar{V} + \pi(1-\delta^2)\, dH$$

The important parameter is the area per unit volume, A/V. In the general case (for any C), $A/V = \alpha C$, where $\alpha = \bar{A}/\bar{V}$. α depends on δ:

$$\alpha = 2\left(\int_{-1}^{1} \frac{dy}{\sqrt{1-y^2}}\sqrt{1+\delta^2+2y\delta}\right)\Bigg/ \left(\int_{-1}^{1} \frac{dy(1+y\delta)}{\sqrt{1-y^2}}\sqrt{1+\delta^2+2y\delta}\right)$$

α decreases from 2 at $\delta = 0$ to 3/2 at $\delta = 1$.

Now consider the surface free energy of a modulated cylinder (with polymer inside). The free energy per unit volume is $F = (A/V)f$, where $f = f(C) = \gamma - \kappa_1 C + 0.5\kappa_2 C^2$ (the κ_G term is irrelevant for an infinite cylinder). Therefore, F is factorized: $F = \alpha(\delta)Cf(C)$, and hence $\min F = \min[Cf(C)]\cdot\max \alpha(\delta)$ (note that $\min[Cf(C)] < 0$; otherwise a cylinder is not stable). Obviously, $\max \alpha(\delta)$ corresponds to $\delta = 0$, so unmodulated cylinder is always more favorable than a modulated one. This statement is also true for inverse cylindrical structures (as can be shown using a similar argument).

Appendix F: The Basic Parameters of Constant Mean Curvature Surfaces

We consider triply periodic surfaces of constant mean curvature including primitive P, diamond D, and gyroid G families. The examples of these surfaces are shown in Figure 5. Each surface can be schematically viewed as roughly cylindrical sections connected into a network with 6-fold (P), 4-fold (D), or 3-fold (G) junctions. The surfaces can be divided in equivalent primitive cells. The natural primitive cell for a P-family surface contains one junction point. For other families (D and G) we consider primitive cells containing two junction points (for D) and four junction points (for G). (The crystallographic unit cells for P and D surfaces contain a number of such primitive cells.) It is convenient to set the primitive cell volume V_{cell} as $V_{cell} = 1$.

The basic parameters of the surfaces are the following: the sum of principal curvatures $C = C_1 + C_2$ which is constant along the surface, the reduced area $\bar{A}$ (the area per primitive cell of unit volume), and the fraction ϕ of the volume enveloped by the surface. $C = 0$ corresponds to a saddle-like minimal surface (primitive P, diamond D, or gyroid G) with $\phi = 1/2$; each minimal surface divide the space in two equivalent subspaces. The reduced areas for the three minimal surfaces are[38,49]

$$\bar{A} \approx 2.3451\ (\mathrm{P}), \quad \bar{A} \approx 2.4177\ (\mathrm{D}), \quad \bar{A} \approx 2.4533\ (\mathrm{G}) \qquad \text{(F1)}$$

The Euler−Poincare characteristic of a surface is

$$n_E = \frac{1}{2\pi}\int C_1 C_2\, \mathrm{d}A$$

According to the Gauss−Bonnet theorem, n_E must take integer values depending on the surface topology (this applies to closed surfaces, and to repeat cells of periodic surfaces). $n_E = -4$ for the defined above primitive cells for P-, D-, and G-family surfaces.

Both the area $A = \bar{A}$ and the curvature $C = \bar{C}$ for the periodic surfaces with primitive cell of unit volume $V_{cell} = 1$ depend only on the volume fraction ϕ (and the topological type of the surface, P, D, or G). The two dependencies ($\bar{A}$ vs ϕ) and ($\bar{C}$ vs ϕ) are connected via the general relationship

$$\mathrm{d}\bar{A} = \bar{C}\,\mathrm{d}\phi \qquad \text{(F2)}$$

The dependencies $\bar{A}(\phi)$ and $\bar{C}(\phi)$ were calculated in refs 38, 49, and 50. The surface/volume and curvature/volume dependencies for the gyroid family are shown in Figure 11 based on the numerical data obtained in both refs 49 and 50. More precisely, we note that the $\bar{C}(\phi)$ dependencies calculated in these papers for gyroid are in perfect agreement (within 1% accuracy), while the agreement for $\bar{A}(\phi)$ is slightly worse. Therefore, we calculated $\bar{A}(\phi)$ using the common $\bar{C}(\phi)$ by integrating eq F2. Thus, obtained $\bar{A}(\phi)$ is in perfect agreement with the more recent numerical data.[50]

Using the numerical data[38,50] obtained for ϕ close to 0.5, we also find the slope $c = -\mathrm{d}\bar{C}/\mathrm{d}\phi|_{\phi=0.5}$ for the three surface families:

$$c \approx 9.45\ (\mathrm{P}), \quad c \approx 8.93\ (\mathrm{D}), \quad c \approx 8.9\ (\mathrm{G}) \qquad \text{(F3)}$$

References and Notes

(1) Flory, P. J. *Principles of Polymer Chemistry*; Cornell University Press: Ithaca, NY, 1971.
(2) de Gennes, P. G. *Scaling Concepts in Polymer Physics*; Cornell University Press: Ithaca, NY, 1985.
(3) Lifshitz, I. M.; Grosberg, A. Yu.; Khokhlov, A. R. *Rev. Mod. Phys.* **1978**, *50*, 683.
(4) Grosberg, A.; Khokhlov, A. *Statistical Physics of Macromolecules*; American Institute of Physics: New York, 1994.
(5) Hamley, I. W. *The Physics of Block-Copolymers*; Oxford University Press: Oxford, England, 1998.
(6) Leibler, L. *Makromol. Chem., Macromol. Symp.* **1988**, *16*, 1.
(7) Aseyev, V.; Hietala, S.; Laukkanen, A.; Nuopponen, M.; Confortini, O.; Du Prez, F. E.; Tenhu, H. *Polymer* **2005**, *46*, 7118.
(8) Inomata, H.; Goto, S.; Saito, S. *Macromolecules* **1990**, *23*, 4887.
(9) Tiktopulo, E. I.; Bychkova, V. E.; Ricka, J.; Ptitsyn, O. B. *Macromolecules* **1994**, *27*, 2879.
(10) Wu, C.; Zhou, S. *Phys. Rev. Lett.* **1996**, *77*, 3053.
(11) Tiktopulo, E. I.; Uversky, V. N.; Lushchnik, V. B.; Klenin, S. I.; Bychkova, V. E.; Ptitsyn, O. B. *Macromolecules* **1995**, *28*, 7519.
(12) Wang, X.; Qiu, X.; Wu, C. *Macromolecules* **1998**, *31*, 2972.
(13) Laukkanen, A.; Valtola, L.; Winnik, F. M.; Tenhu, H. *Macromolecules* **2004**, *37*, 2268.
(14) Akiyoshi, K.; Kang, E.-C.; Kurumada, S.; Sunamoto, J.; Principi, T.; Winnik, F. M. *Macromolecules* **2000**, *33*, 3244.
(15) Vasilevskaya, V. V.; Khalatur, P. G.; Khokhlov, A. R. *Macromolecules* **2003**, *36*, 10103.
(16) Laschewsky, A. *Adv. Polym. Sci.* **1995**, *124*, 1.
(17) Leibler, L.; Orland, H.; Wheeler, J. *J. Chem. Phys.* **1983**, *79*, 3550.
(18) Halperin, A. *Macromolecules* **1987**, *20*, 2943.
(19) Rubinstein, M.; Colby, R. H. *Polymer Physics*; Oxford University Press: Oxford, UK, 2003.
(20) Zhang, L. F.; Eisenberg, A. *Science* **1995**, *268*, 1728.
(21) Zhulina, E. B.; Adam, M.; LaRue, I.; Sheiko, S. S.; Rubinstein, M. *Macromolecules* **2005**, *38*, 5330.
(22) Nyrkova, I. A.; Semenov, A. N. *Eur. Phys. J. E* **2005**, *17*, 327.
(23) Zhang, G. Z.; Wu, C. *Phys. Rev. Lett.* **2001**, *86*, 822.
(24) Gorelov, A. V.; Du Chesne, A.; Dawson, K. A. *Physica A* **1997**, *240*, 443.
(25) McPhee, W.; Tam, K. C.; Pelton, R. *J. Colloid Interface Sci.* **1993**, *156*, 24.
(26) Wu, C.; Zhou, S. *Macromolecules* **1995**, *28*, 8381.
(27) Jarkova, E.; Johner, A.; Maresov, E. A.; Semenov, A. N. *Eur. Phys. J. E* **2006**, *21*, 371.
(28) Ushakova, A. S.; Govorun, E. N.; Khokhlov, A. R. *J. Phys.: Condens. Matter* **2006**, *18*, 915.
(29) Lau, K. F.; Dill, K. A. *Macromolecules* **1989**, *22*, 3986.
(30) Lau, K. F.; Dill, K. A. *Proc. Natl. Acad. Sci. U.S.A.* **1990**, *87*, 6388.
(31) Eigen, M.; Winkler-Oswatitsch, R. *Steps Towards Life: a Perspective on Evolution*; Oxford University Press: Oxford, UK, 1992.
(32) Shakhnovich, E. I.; Gutin, A. *Biophys. Chem.* **1989**, *34*, 187.
(33) Shakhnovich, E. I.; Gutin, A. M. *Proc. Natl. Acad. Sci. U.S.A.* **1993**, *90*, 7195.
(34) Pande, V. S.; Yu.Grosberg, A.; Tanaka, T. *Proc. Natl. Acad. Sci. U.S.A.* **1994**, *91*, 12976.
(35) Li, H.; Helling, A.; Tang, C.; Vingreen, N. *Science* **1996**, *273*, 666.
(36) Sfatos, C. D.; Shakhnovich, E. I. *Phys. Rep.* **1997**, *288*, 77.
(37) Grosberg, A. Yu. *Usp. Fiz. Nauk (Russ. Phys. Usp.)* **1997**, *167*, 129.
(38) Anderson, D. M.; Davis, H. T.; Nitsche, J. C. C.; Scriven, L. E. *Adv. Chem. Phys.* **1990**, *77*, 337.
(39) Anderson, D. M.; Thomas, E. L. *Macromolecules* **1988**, *21*, 3221.
(40) Hajduk, D. A.; Harper, P. E.; Gruner, S. M.; Honeker, C. C.; Kim, G.; Thomas, E. L.; Fetters, L. J. *Macromolecules* **1994**, *27*, 4063.
(41) Schwarz, H. A. *Gesammelte Mathematische Abhundlungen*; Springer: Berlin, 1890.
(42) Schoen, A. H. Infinite Periodic Minimal Surfaces Without Self-Intersections, NASA Technical Report D5541, 1970.
(43) Terrones, H. *Colloq. Phys.* **1990**, *C7*, 345.
(44) Andersson, S.; Hyde, S. T.; Larsson, K.; Lidin, S. *Chem. Rev.* **1988**, *88*, 221.
(45) Likhtman, A. E.; Semenov, A. N. *Macromolecules* **1997**, *v.30*, 7273.
(46) Khandpur, A. K. *Macromolecules* **1995**, *28*, 8796.
(47) Matsen, M. W.; Bates, F. S. *Macromolecules* **1995**.
(48) Dubois-Violette, E.; Pansu, B., Eds. International workshop on geometry and interfaces (Aussois, France); *J. Phys. Colloq.*, **1990**, *C7*.
(49) Grosse-Brauckmann, K. *J. Colloid Interface Sci.* **1997**, *187*, 418.
(50) Jung, Y. K.; Chu, S.; Torquato, J. *Comp. Phys.* **2007**, *223*, 711.
(51) Helfrich, W. *Z. Naturforsch.* **1973**, *28c*, 693.
(52) Landau, L. D.; Lifshitz, E. M.; Pitaevskii, L. P. *Physical Kinetics*; Butterworth-Heinemann: London, 1997.
(53) Semenov, A. N. *Macromolecules* **1993**, *26*, 2273.
(54) Kujawa, P.; Aseyev, V.; Tenhu, H.; Winnik, F. M. *Macromolecules* **2006**, *39*, 7686.
(55) Balu, C.; Delsanti, M.; Guenoun, P. *Langmuir* **2007**, *23*, 2404.
(56) Chan, K.; Pelton, R.; Zhang, J. *Langmuir* **1999**, *15*, 4018.

(57) Khokhlov, A. R.; Semenov, A. N.; Subbotin, A. V. *Eur. Phys. J. E* **2005**, *17*, 283.
(58) Semenov, A. N. *Macromolecules* **2004**, *37*, 226.
(59) Semenov, A. N.; Joanny, J.-F.; Khokhlov, A. R. *Macromolecules* **1995**, *28*, 1066.
(60) Leibler, L. *Macromolecules* **1980**, *13*, 1602.
(61) Hennaux, P.; Laschewsky, A. *Colloid Polym. Sci.* **2001**, *279*, 1149.
(62) Borisov, O. V.; Halperin, A. *Macromolecules* **1996**, *29*, 2612.
(63) Borisov, O. V.; Zhulina, E. B. *Macromolecules* **2005**, *38*, 2506.
(64) As an example, consider the regime $\epsilon \ll k_BT$ and $|B + B'| \ll \epsilon/k_BT\psi_0$: here $\gamma \simeq \gamma_0 - k_BT\psi_0 l\epsilon/4$ (see eq 31), so γ vanishes for $l \sim na_Hk_BT/\epsilon$ (as $\psi_0 = c_0/n$, $\gamma_0 \sim k_BTc_0a_H$). In this regime, the polymer phase can be stable against microphase separation even at $\gamma = 0$ (see eqs D1 and D3; these equations are compatible with the conditions mentioned above).
(65) See condition (36). We focus on the regimes where this condition is respected, so L_{ref} is indeed much larger than the monomer size l, $L_{ref} \gg l$. This is true, for example, for $\epsilon \ll k_BT$ and $|B - B'| \ll (1/\psi_0)(\epsilon/k_BT)$ (see eq 29).
(66) Dobrynin, A. V.; Rubinstein, M.; Obukhov, S. P. *Macromolecules* **1996**, *29*, 2974.
(67) Landau, L. D.; Lifshitz, E. M. *Statistical Physics*; Pergamon Press: Oxford, 1998.
(68) Globule is a compact state of a single polymer chain. Mesoglobule is an aggregate of several polymer chains.
(69) We make the following distinction between micelles and globules (mesoglobules). Micelle is a relatively small object: its size is defined by the size of polymer repeat unit (for example, the size of side chain in the case of grafted amphiphilic copolymer or block size in the case of block copolymer). Typically, micelles have well-segregated core/shell structure (with hydrophobic parts in the core and hydrophilic in the shell). Globules (and mesoglobules incorporating more than one polymer chain) are larger and typically consist of a nearly homogeneous core where solvophobic and solvophilic units can be mixed (the core may also exhibit a microdomain structure; this more complicated case is not considered here) and a relatively thin surface layer where solvophilic units are dominating.
(70) $c_H \approx$ const in the core, including the inner l-layer (see Figure 3), since the volume fraction of P-subunits is small, so the presence of grafted subunits does not affect much the conformation of H-backbone. The condition $c_H \approx$ const is also discussed; see section 4.1.
(71) Note that, strictly speaking, equilibrium concentration inside a globule differs from that in the macroscopic bulk polymer phase. However, the difference, which is due to the surface curvature effects (Laplace pressure), is extremely small for large globule in the region of interest (when surface tension is nearly vanishing). For this reason the chemical potential μ can be considered as a constant corresponding to the macroscopic polymer phase.
(72) The same conclusion can be expressed in more "mathematical" terms: the three saddle-like minimal surfaces (P, D, and G) are all related by the theoretical transformations, the Bonnet transformations. The transformations conserve the local properties of the surface, including area and curvature (both mean and Gaussian). Therefore, the surface free energies (per primitive cell) of Bonnet-related surfaces are exactly the same. The only important parameter that changes is the cell volume, which turns out to be the smallest for the gyroid morphology; hence, its negative free energy per unit volume of condensed polymer is the highest.

MA801260G